CERN-SND@LHC-NOTE-2023-001
May 18, 2023

Measurement of the muon flux at SND@LHC

S. Ilieva Ilieva[1],

Abstract

The Scattering and Neutrino Detector at the LHC (SND@LHC) is a compact standalone experiment, which started taking data at the beginning of Run 3 of the LHC. The experiment is designed to perform measurements with high-energy neutrinos in range 100 GeV–1 TeV produced at the LHC in a previously unexplored pseudo-rapidity range of $7.2 < \eta < 8.4$. The detector, located 480 m downstream of the ATLAS interaction point in the TI-18 tunnel, comprises a hybrid system based on an 800 kg target mass of tungsten plates, interleaved with emulsion and electronic trackers, followed downstream by a calorimeter and a muon system. The first electronic detector measurement of the muon flux in the TI-18 tunnel, using the SciFi tracker and downstream muon detector, is reported here. The geometrical acceptance of the downstream muon detector exceeds and fully covers the SciFi one. The measured muon flux through a $31{\times}31$ cm^2 central SciFi area is

$$2.06 \pm 0.01(\text{stat}) \pm 0.11(\text{sys}) \times 10^4\,\text{fb/cm}^2,$$

while for the downstream muon system the flux is

$$2.35 \pm 0.01(\text{stat}) \pm 0.08(\text{sys}) \times 10^4\,\text{fb/cm}^2$$

for a $52{\times}52$ cm^2 central detector area. The total relative uncertainty of the results is 5 % for the SciFi and 3 % for the DS measurement. The Monte Carlo simulation prediction of these fluxes is 20-25 % lower than the measured values.

[1] *Università di Napoli "Federico II", Napoli, Italy*

VERSION	DATE	COMMENTS
01	02.10.2022	First version

Contents

1 Motivation

The majority of recorded events in the SND@LHC detector consist of long-range muons produced in proton-proton collisions at the ATLAS interaction point, henceforth referred to as IP1 following the LHC convention. Besides detector response studies and calibration, muons penetrating the full detector possess two analysis purposes. First, it is the measurement of the muon flux at the SND@LHC location, i.e. in a very forward rapidity range. Second, the muon flux measurement is also important since muons reaching the detector location are the main source of background for the neutrino search. Muons can either enter the detector without being vetoed and generate showers via bremsstrahlung or deep inelastic scattering, or interact in the surrounding material and produce neutral hadrons entering the apparatus and possibly mimicking neutrino interactions. The muon flux measurement is the subject of the current note.

2 Detector description

2.1 Apparatus

The SND@LHC detector [1] is designed to perform measurements with high energy neutrinos (100 GeV–1 TeV) produced at the LHC in the forward pseudo-rapidity region $7.2 < \eta < 8.4$. It allows the identification of all three flavours of neutrino interactions with high efficiency.

SND@LHC is a compact hybrid apparatus, shown in Figure 1.

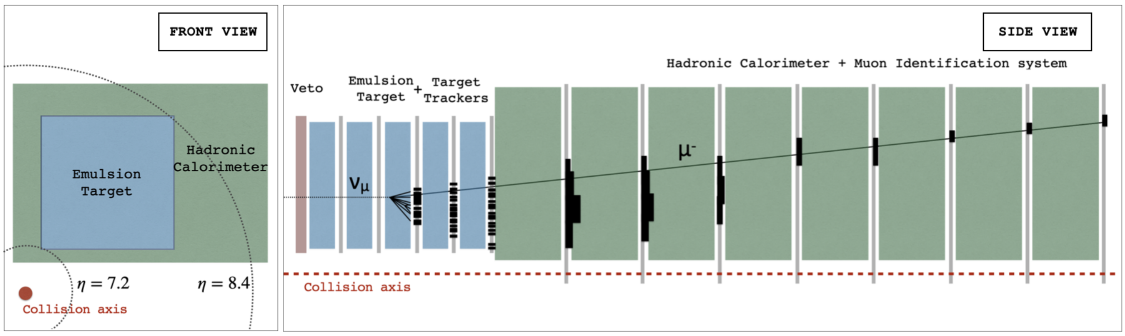

Figure 1: Layout of the SND@LHC detector.

It consists of three parts: veto, target and muon systems. The veto detector (Veto) is situated in front of the target region. It is made of two planes, with a relative shift vertically with respect to one another, of seven vertically stacked $42 \times 6 \times 1$ cm^3 scintillating bars. The Veto tags the passage of charged particles, which are mostly muons from IP1. The target section contains five walls. Each wall consists of four units of emulsion cloud chambers (ECC) and it is followed by a Scintillating Fibre tracker (SciFi) station. The muon system is placed downstream of the target. The electronic detectors, Veto, SciFi and muon systems, provide the time stamp of the neutrino interaction, preselect the interaction region, measure the energy of electromagnetic and hadronic showers, and identify muons.

The sub-micrometric precision of nuclear emulsions allows the detection of short-lived particles like tau leptons. Each ECC module is a sequence of 60 emulsion films, 19.2×19.2 cm^2, interleaved with 59 tungsten plates, 1 mm thick. Its weight is approximately 41.5 kg, adding up to 830 kg for the total target mass. The tungsten plates in one brick amount to about 17 radiation lengths, X_0, or about 85 X_0 for the whole target. Each SciFi station consists of two 39×39 cm^2 x-y planes of staggered scintillating fibres with a diameter of 250 μm. The fibres are arranged in six densely-packed staggered layers, forming fibre mats of 1.35 mm thickness. Each mat is 13 cm wide and 39 cm long. Three fiber mats are integrated into a fibre plane, with less than 500 μm dead zones. The spatial resolution of single hits, about 150 μm, is sufficient to link hits with an interaction in an ECC. The data from the ECC is not used for the analysis described in this note.

The muon system consists of two parts: upstream (US), the first five stations, and downstream (DS), the last three stations. In combination with SciFi, it acts as a coarse sampling calorimeter ($\sim$ 9.5 λ_{int}), providing the energy measurement of hadronic jets. Each US station consists of 10 vertically stacked scintillator bars of $82.5 \times 6 \times 1$ cm^3, similar to the upstream veto detector. Each DS station consists of two layers of thin bars, one horizontally and one vertically arranged, allowing for a spatial resolution less than 1 cm and acting as Muon Identification system. The most downstream DS station has an additional plane of horizontally stacked bars. The DS stations are interleaved with 20 cm thick iron blocks. Each of the latter is equivalent to 11 X_0, or 33 X_0 in total for the whole DS system.

The readout electronics for the SciFi are arrays of silicon photomultipliers (SiPMs) which are glued to the fiber mats. The Veto and the muon system bars are also read out using SiPMs technology. For Veto and US bars, 8 SiPMs are reading the signal on each side of their horizontal bars. The signal in DS vertical bars is collected by a single SiPM on the top, while horizontal bars are readout by one SiPM on each side.

In many instances throughout the current note the short acronym denoting each system (Veto, SciFi, US, DS) is combined with a number indicating the Veto, SciFi, or the downstream muon system plane. For example, Veto 1, Veto 2, SciFi 1, .., SciFi 5, US 1, .., US 5, DS 1, .., DS 4. The convention is the numbering of each system's planes and stations starts from the front of the detector, i.e. left to right on Figure 1. Additionally, the position of the electronic readout for a given detector element is indicated using L for left- and R for right-hand side readout position with the line-of-sight direction being from Veto to DS.

2.2 Detector location and coordinate system

The SND@LHC detector is placed in the TI-18 service tunnel that was initially constructed for injection of positrons from the SPS to the LEP accelerator. The schematic in Figure 2 describes the detector location in the accelerator area. The position is between the ATLAS interaction point (IP1), which is 480 m away, and the ALICE

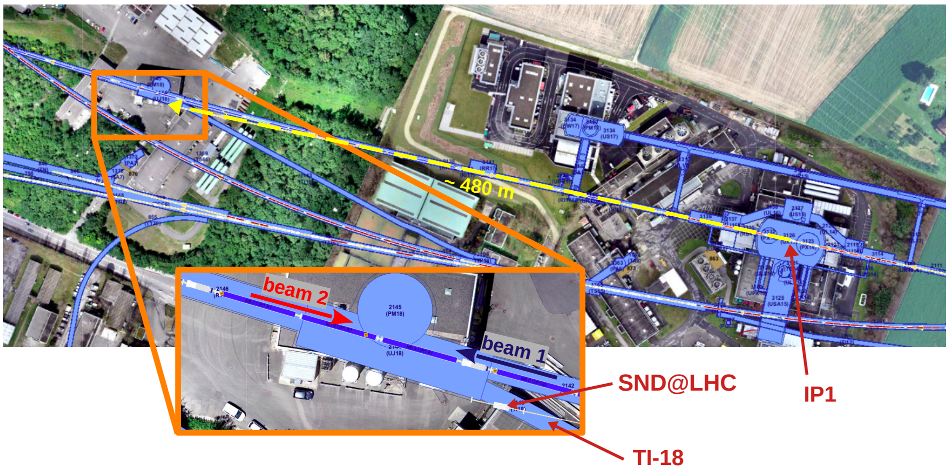

Figure 2: The location of the SND@LHC detector in the LHC complex area. The apparatus is located in the TI-18 tunnel, 480 m away from IP1. The directions of the two circulating beams, Beam 1 (blue) and Beam 2 (red) are shown in the zoomed panel. Beam directions and colors follow the convention used in Reference [2].

IP (IP2), which is more than 2 km away from the detector. Given the closer proximity and the much higher luminosity compared to IP2, beam crossings at IP1 are by far the dominant source of particles reaching the detector.

For every LHC fill a well-defined bunch structure, also noted as LHC filling scheme, is available at the LHC Programme Coordination web page [3]. The filling scheme specifies which bunches cross at different interaction points and which bunches of Beam 1 and Beam 2 are circulating in the LHC without collision. It is a common convention that the clock-wise circulating beam is denoted Beam 1, while the counter clock-wise circulating one is Beam 2 [2]. Only after the bunches have been accelerated to the target energy and the LHC enters the "Stable beams" operation stage [4], bunches are brought to collision.

The information regarding the LHC bunch structure is synchronized with the SND@LHC event timestamp. The phase adjustments for both beams are done by finding the phase shift with maximum overlap with SND@LHC event rates. For Beam 1, it means matching the highest event rates to IP1 collisions. The synchronized bunch structure provides input on whether an event is associated with IP1 collisions. However, circulating beam particles can eventually interact with the machine elements, independent of whether the particle is in a colliding bunch or not. The filling scheme allows unambiguously to identify events originating from Beam 1 which was not colliding in IP1, and Beam 2 which was not colliding in IP2.

The coordinate system adopted by the SND@LHC collaboration is presented in Figure 3. Its origin, the DCUM.480, is on the IP1 beam collision axis, 480 m away from IP1. The Z axis is aligned with the beam collision axis, the LHC machine axis at IP1, and points from IP1 towards the TI-18 tunnel. The Y axis is perpendicular

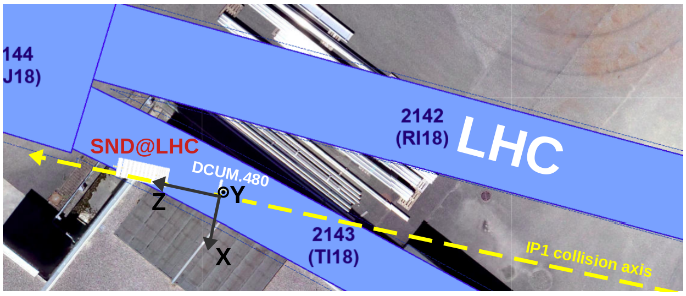

Figure 3: The SND@LHC coordinate system. The origin is noted DCUM.480 and is 480 m away from IP1. The Z axis is aligned with the IP1 beam collision axis for null crossing angle. The Y axis is perpendicular to the LHC machine plane and points upwards. The X axis is perpendicular to Y and Z and points away from the LHC center.

to the LHC machine plane and points upwards. The X axis is perpendicular to Y and Z and points away from the LHC center, as to have a right-handed coordinate system. In this coordinate system the $y - z$ plane contains local gravity and is the vertical plane, while the perpendicular $x - z$ plane is the horizontal one.

3 Data

The LHC Run 3 commissioning proton-proton collisions at 450 GeV served to confirm that the detector is operating as expected and traversing muons, other than cosmic-ray muons, can be successfully reconstructed. The detectors were running for the first LHC Run 3 proton-proton collisions at 13.6 TeV on July 5, 2022, and were taking data until the end of 2022. Detector operation has mostly been smooth and issues identified and sorted out promptly.

During the complete LHC proton run at 13.6 TeV, the recorded integrated luminosity for SND@LHC 2022 run is 36.8 fb^{-1}. It comprises 95% of the total 38.7 fb^{-1} delivered luminosity at IP1 reported by the ATLAS collaboration [5, 6]. After the end of the proton-proton run on November 28, 2022, the last batch of emulsions was extracted. Still, the electronic detectors kept recording events during the following LHC ion run and continue operation as of now.

For this analysis, data collected during proton-proton collisions at 13.6 TeV energy, and "Stable beams" mode of the LHC accelerator are used. Two SND@LHC runs are selected. Information about them is outlined in Table 1. It includes the LHC fill number, integrated luminosity, mean number of inelastic pp collisions per bunch crossing, run number, number of recorded events, the date and duration for each run.

The run selection is based on event counts and the LHC filling scheme. The latter is important since it allows to identify muons from different origins which enter the detector depending on the passing beam direction and presence of proton-proton collisions. Muons penetrating the detector originate in IP1 collisions, as well as Beam 1 and Beam 2 interacting with the LHC machine elements or residual gas.

LHC fill number	L_{int} $[fb^{-1}]$	mean $N_{\text{interactions}}$ per bunch crossing	SND@LHC run number	N_{events} $[10^6]$	date, year 2022	duration $[h]$
8088	0.337	35.2	4705	71	3 Aug	12.5
8297	0.529	45.4	5086	101	20 Oct	19.8

Table 1: List of selected SND@LHC 2022 data runs. The runs are chosen to have large event counts, high delivered luminosity, isolated LHC bunches of Beam 2 passing without collisions, and different LHC filling schemes.

The filling scheme for LHC fill 8297 is a mixed one with alternated 25-ns bunch trains and 8 bunches and 4 empty slots (8b4e) trains. It suppresses the formation of electron cloud in LHC arcs and reduces beam-gas interactions [7]. The goal of the current analysis is the measurement of the muon flux at the SND@LHC detector that is associated with proton-proton collisions at IP1 and at LHC's top energy of 6.8 TeV per beam. The contributions of Beam 1 and Beam 2 interacting with the LHC machine elements or residual gas have to be subtracted from the total number of recorded muons. This is done using the filling scheme to identify Beam 1 passing with no IP1 collisions, and Beam 2 passing with no IP1 collisions. The selected runs, see Table 1, correspond to LHC fills with comparatively large isolated non-colliding Beam 2, and also non-colliding Beam 1, bunches, to facilitate extraction of their contribution.

The muon flux at the SND@LHC detector is estimated using emulsion data too. Emulsion runs are divided into groups following emulsion walls installation and extraction dates. A separate note treats the first emulsion data muon flux measurement [8].

4 Simulations

Apart from the data-driven tracking efficiency evaluation, simulations are used to estimate the Monte Carlo track reconstruction efficiency. Generally, the Monte Carlo simulation consists of two stages. The first step combines the generation of proton-proton collisions at the IP1 and the propagation of collision debris in the accelerator tunnel to a virtual scoring plane in the rock tens of meters upstream of the SND@LHC apparatus. The second stage includes particle transport through the rock and the detector.

The first step is carried out by CERN's SY-STI team using Fluka [9, 10]. The DPMJET event generator [11, 12] is used to simulate pp collisions at 13.6 TeV. The proton beams crossing angle is accounted for in the simulation. The proton beams cross in IP1 with a half-angle of about 150 microradians, either upwards(positive angle) or downwards(negative angle) in the vertical plane. In the year 2022 LHC run, that angle was -160 μrad. In the upward/downward configuration, the beam axis as seen in TI-18 gets vertically displaced up to 8 cm above/below the ATLAS detector axis [1].

Particle transport in the LHC is done using the LHC FLUKA model [13, 14]. It has a detailed tunnel description and is being constantly improved. The simulations for the SND@LHC experiment do not feature the ATLAS solenoid magnet, i.e. particles produced in IP1 collisions go through the ATLAS cavern that does not include the detector, but only the vacuum chamber and the forward shielding. On the other hand, the model of the LHC magnetic fields is essential for the SND@LHC Monte Carlo simulation muon rate studies. Muons and anti-muons can be deflected towards or away from the detector acceptance. Recently, the SY-STI team has extended the description of the LHC magnetic field including the magnetic field map in the yoke of the recombination dipole (D2) and the matching section quadrupoles (Q4 to Q7). This implementation, together with the inclusion of the tight setting of the TCL6 physics debris collimator (1 mm half-gap) adopted in the 2022 run, has brought the MC simulation prediction and the SND@LHC electronic detector muon flux measurement to a much better agreement than previously observed: a factor of 2 reduction of the predicted flux is obtained following the magnetic field map expansion and the TCL6 collimator tightening. For this reason when making data/simulation comparisons in Section 9, two MC simulation sets are being considered, one before and one after adjusting the simulations to the actual experimental conditions as far as beam crossing angle, collimator settings, and magnetic field range are concerned. The differences between these two MC simulation samples are outlined in Table 2. These are the number of generated proton-proton collisions, scoring plane size, the beam crossing angle, the TCL6 gap, and the magnetic field map coverage. In both cases the scoring plane is centered on the ATLAS detector axis. Regardless of the larger surface of the first plane, they both cover the spatial area which contributes the most to the muon rate at the location of the detector.

date produced	number of pp collisions [10^6]	scoring plane size [m^2]	beam crossing angle [μrad]	TCL6 half-gap [mm]	magn. field map coverage
March 2022	10	2.5×2.5	-150	2	-
March 2023	200	1.8×1.8	-160	1	extended

Table 2: Overview of the two FLUKA samples of muons from IP1 proton-proton collisions that are used for the data/MC simulation comparison in Section 9. The number of generated pp collisions, the scoring plane size, the beam crossing angle, the TCL6 collimator settings, and the magnetic field coverage differ. The March 2023 set is preceded by a smaller 50-million pp collisions set that indicates the better agreement between data and MC simulation. Afterwards the larger-statistics simulation sample has been generated by the CERN SY-STI and provided to the SND@LHC collaboration.

The FLUKA particle transport is stopped at a virtual scoring plane where positions and momenta of muons are recorded together with their statistical weight, which is different from 1 because of the use of convenient biasing techniques, and information on the muon history. For the latest FLUKA sample, the plane has dimensions 1.8×1.8 m^2. It is located 60 m upstream of the TI-18 tunnel in order to decouple muon interactions in rock and concrete upstream of the detector from the primary flux of muons produced at the IP and within LHC machine elements.

The second stage of the simulation chain is carried out by the SND@LHC team. The FLUKA simulation output serves as input for a GEANT4 [15] particle transport to and through the detector. Not all primary muons, i.e., muons recorded at the scoring plane, enter the detector. Also, primary muons can interact along the way and initiate new particle production. All generated particles are propagated through the rock upstream of the detector, then the TI-18 tunnel and the detector volume. It is found that particles produced by a primary muon more than 10 m upstream of the apparatus do not reach it.

After the simulation event sample is produced, the particle's energy loss in the SND@LHC sensitive detectors, SciFi fibers and veto and muon system bars, is digitized. The light propagation and attenuation inside the scintillators are taken into account. If several particles have passed through a sensitive volume in the same event, the sum of their energy deposit and the timing of the earliest entering particle are assigned to the digitized hit charge and time. Additionally, each hit's timing information is smeared using the detector time resolution of a few hundred of picoseconds [16]. For SciFi, the known conversion of energy to number of photoelectrons, and a signal threshold check are applied. Per detector element with non-zero deposited energy, there is one digitized hit assigned to the corresponding readout channel. If the readout of the element is realized on more than one SiPM channels, the signal is equally divided between SiPMs. This is the case for the horizontal bars in the muon system. It is important to note that track finding is based on the coordinates of the fired detector elements. Besides the hit's signal threshold and unless otherwise imposed, tracking is independent of the charge and arrival time hit attributes.

5 Detector spatial and time alignment

The SciFi spatial alignment is made by minimizing the residuals of the muon trajectory with respect to the measurements used. The event selection for this procedure requires at least 10 measurements and a converged track fit using at least 8 measurements. The residual is calculated using the distance of closest approach between a SciFi track and a fired detector element. The SciFi detector consists of 5 stations and each of them is made of a horizontal and a vertical plane, with 3 mats of fibres in each plane. The alignment parameters used are the relative mat positions in the measurement plane and the rotation angles for the whole plane, see Figure 4. The procedure is not sensitive to the Z position. The initial positions are taken from the survey [17], which have a precision of about 1 mm. For each projection, in two of the planes the position of one mat is fixed, since the procedure cannot determine the global alignment of the SciFi detector within the TI-18 tunnel. The rotation of one plane is fixed. The alignment is done after each emulsion replacement. The procedure uses an iterative approach by running the SIMPLEX algorithm of Minuit by minimizing the residuals of the fitted track and its measurements. The final residuals have a spread of typically 150 - 200 µm, larger than expected from the

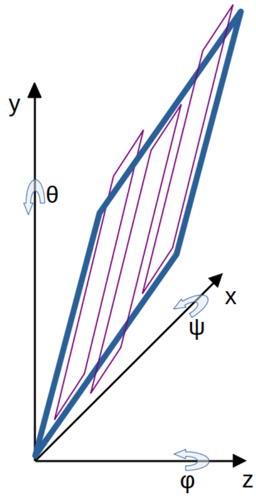

Figure 4: A schematic of a SciFi plane (blue titled square) comprising 3 mats (violet tilted rectangles). The SciFi spatial alignment procedure determines the relative positions of the mats in the plane and the rotation of the whole plane.

pure detector resolution [16] due to the material between stations and large multiple scattering. Figure 5 presents the residuals per mat before and after spatial alignment.

The SciFi time alignment is done using the timing of measurements used for a SciFi track fit. The time is corrected for the signal speed knowing the particle impact point from the particle trajectory. A velocity of 15 cm/ns is assumed [16]. In the first step, each station is time aligned internally. The channels within a SciFi mat are already well aligned. For each station, there are 2×3 time constants (two planes, each plane made of 3 mats) to be determined and 9 available time difference measurements for each combination of mats, see Figure 6a. The time constant for mat 0 of the horizontal plane is set to zero. Minuit is used to find the best solution for the other 5 constants. In the second step, the time alignment between the stations is determined by correcting for the time of flight of the particle. The average internal aligned time of a X and Y track measurement in a plane is used. There are 5 time constants to be determined and 10 time differences between stations available from the data, see Figure 6b. The time constant of the first station is set to zero, and Minuit is again used to get the best solution from the 10 mean differences between stations. Figure 7 shows an example of the timing residuals between SciFi stations 1 and 2, noted Δt on the plots, before and after time alignment. The data on each plot is fitted with a Gaussian and its width corresponds to about 250 ps time resolution per station.

The DS spatial alignment is done minimizing the residuals of DS hit positions with respect to extrapolated SciFi tracks. Since SciFi stations are moved for emulsion extractions, even though the DS stations are stationary during all runs, the DS spatial alignment is re-done. Figure 8 is an example plot of DS X residuals before and after the alignment. In the presented case, the reference plane, where SciFi tracks are extrapolated to and their positions are compared to DS hits, is the

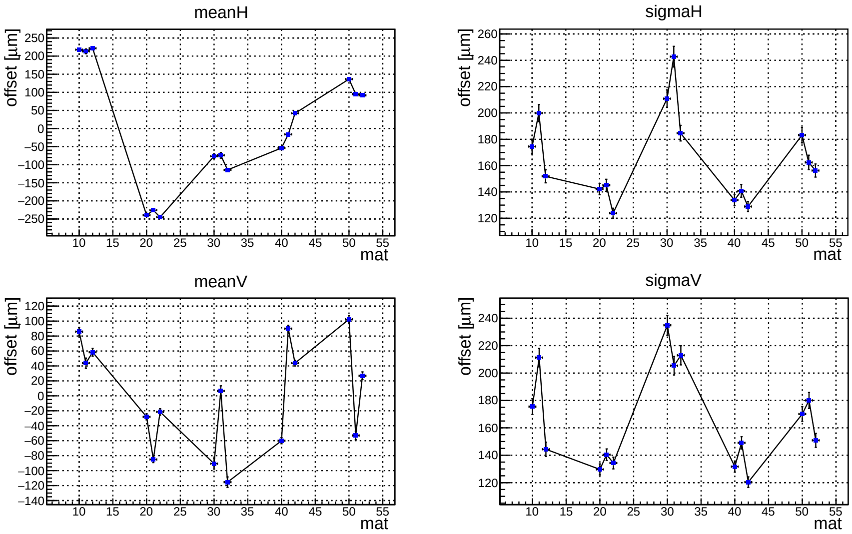

(a)

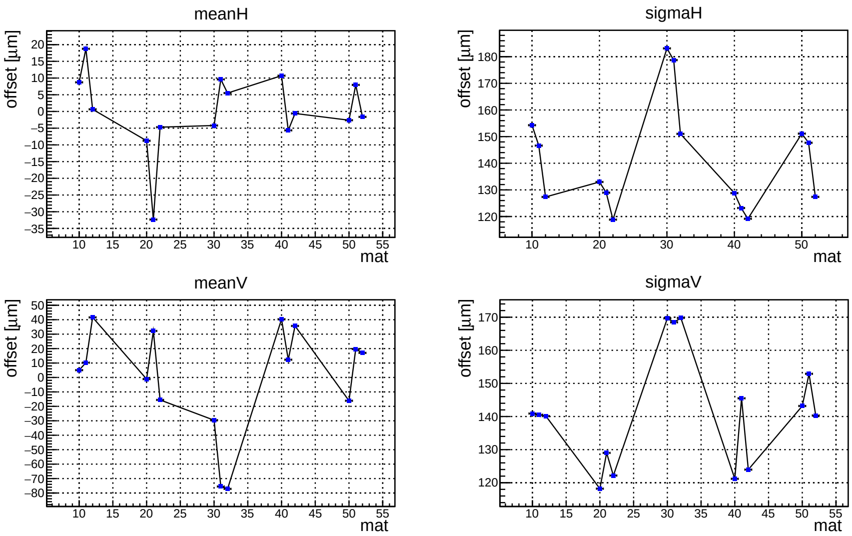

(b)

Figure 5: SciFi residuals before (a) and after (b) spatial alignment. Per horizontal (H) and vertical (V) projection there are the mean and widths of residual distributions per mat. For each plot, the abscissa label denotes the station by the tens of the number and the mat by the units. The top-panel plot is obtained using 1M events, while the bottom-panel one is for the full run. After the alignment residuals between tracks and measurements are significantly reduced. The vast majority of them have less than a 150-micrometer spread. Data from SND@LHC run 4705.

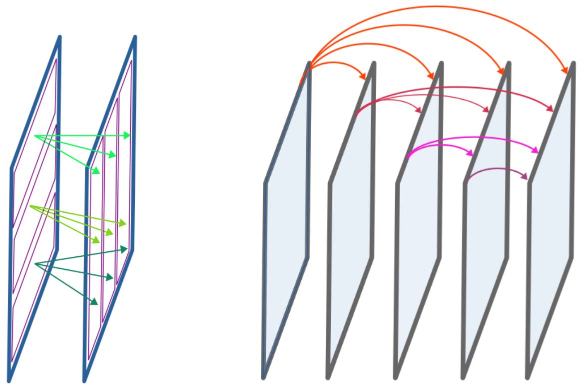

(a) (b)

Figure 6: A diagram showing all mat combinations used for the internal time alignment of a SciFi station (a) and the station combinations used for the time alignment of the full SciFi detector (b). The arrows on each plot indicate the time difference measurements which are used in the alignment procedure. On plot (a), SciFi mats are depicted as violet tilted rectangles, while the two planes of horizontally and vertically staggered mats building up a station are presented as blue tilted squares. On plot (b), the 5 SciFi stations are depicted as tilted grey squares.

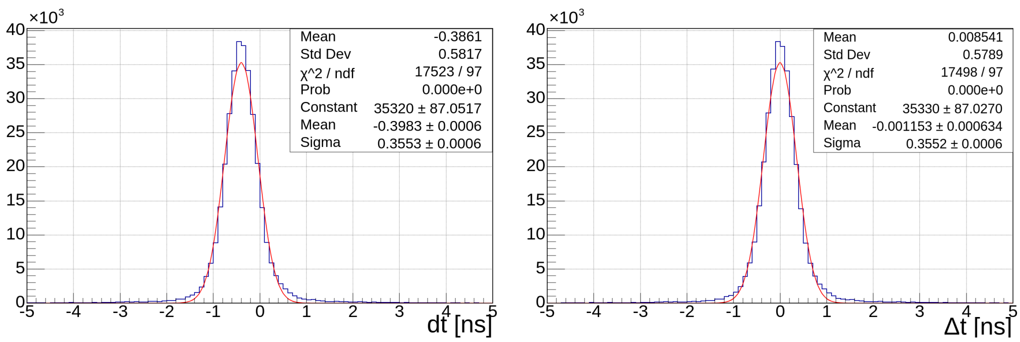

(a) (b)

Figure 7: SciFi timing residuals between measurements in station 1 and 2 before (a) and after (b) time alignment. After the alignment, the residuals are symmetrically centered around 0. Each distribution is fitted with a Gaussian function. Its width corresponds to a 250 ps time resolution per station. Data from run 4705.

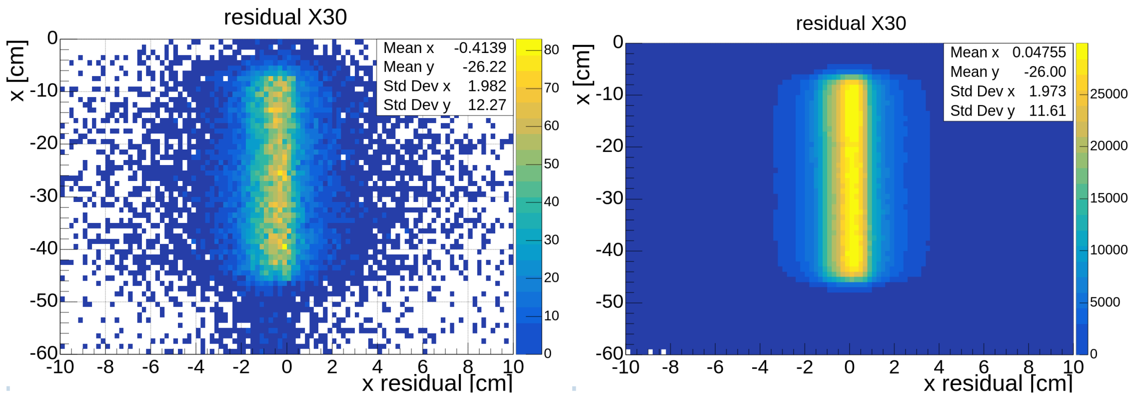

(a) (b)

Figure 8: DS X residuals at the vertical DS 1 plane vs X position before (a) and after (b) spatial alignment. The left-panel plot is obtained using 1M events, while the right-panel one is for the full run. After the alignment, X residuals are reduced by a centimeter and symmetrically centered around 0. Data from run 4705.

vertical DS 1 plane.

The DS time alignment is done with respect to SciFi tracks. The latter are extrapolated to each DS plane. The timing residuals between a matched DS plane hit and the extrapolated track prediction are minimized. The timing residual, Δt, is defined as

$$\Delta t = t_{DS\ hit} - t_{sc.\ light} - L/c - t_{SciFi\ ref}. \tag{1}$$

The time of the recorded DS hit is $t_{DS\ hit}$. The time of flight, L/c, between SciFi track's reference start position and the DS plane, assuming the particle's velocity $v = c$, is subtracted. The muon making the SciFi track crossed the reference start position at a time denoted $t_{SciFi\ ref}$. The reference start position is SciFi 1. The time for scintillation light propagation inside a fired bar, $t_{sc.\ light}$, is also accounted for. The light propagation speed along a DS bar is 15 cm/ns [16]. It is found that the DS time alignment is possible by applying a linear correction with a single slope and custom offsets per half-plane and readout side. Then, the time correction is applied per readout channel. The timing residuals after DS time alignment are shown on Figure 9.

6 Tracking

Tracking in the SND@LHC electronic detectors is performed independently in two detector sub-systems, the SciFi and the DS of the muon system. The Upstream Stations of the muon system are not considered for track building because of their large transverse dimension of 6×1 cm^2. One argument for treating SciFi and DS as separate trackers is the much different granularity of their sensitive elements. While the DS transverse bar dimensions are 1×1 cm^2, the width of the SiPM channels reading the SciFi fiber mats is only 250 μm. Another reason is that by construction

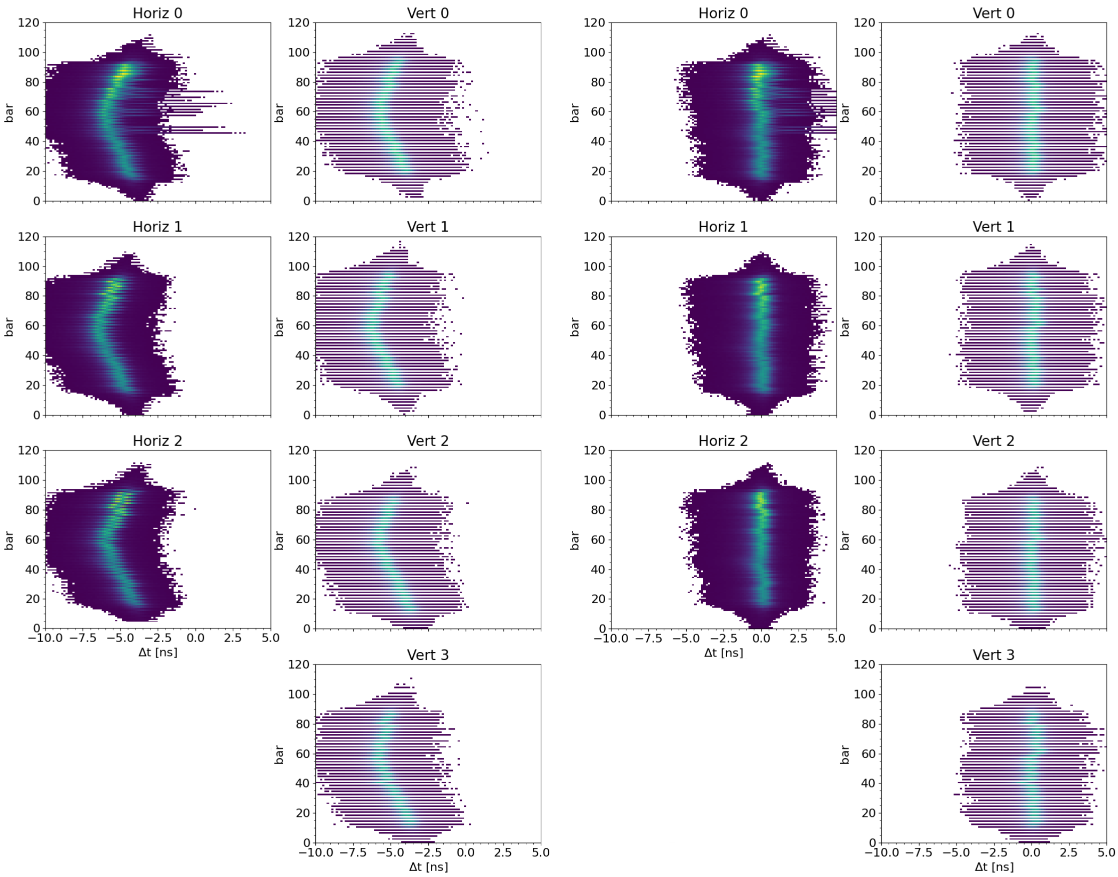

(a) (b)

Figure 9: The timing residuals before (a) and after (b) DS time alignment. The timing residuals are defined in Equation 1. For horizontal DS planes, readout channels on the left detector side are noted using odd numbers, while even ones are reserved for right-side SiPMs. Vertical DS planes are readout only on the top, which is designated using odd numbers. Before time alignment, specific curved structures are clearly observable for each plane. They originate from differences in the routing of bar readout signals. All distributions are centered at $\Delta t = 0$ ns after the alignment. Data from run 4705.

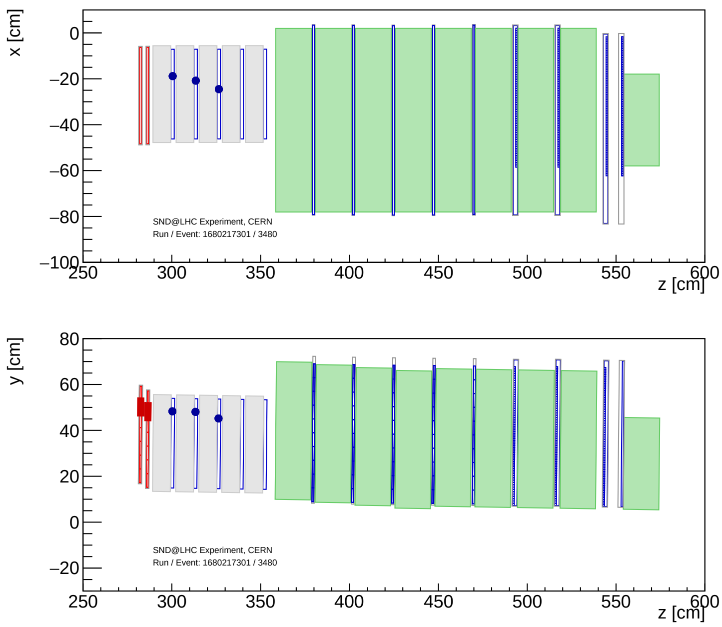

Figure 10: SND@LHC 2D event display of a simulated event where a 0.6 GeV muon is absorbed in the target region of the detector. The top panel shows the horizontal XZ plane, while the bottom one shows the vertical YZ plane.

the DS acceptance is 2.4 times larger than the SciFi one, with the DS fully covering the SciFi acceptance.

Most long-range muons traveling from IP1 towards the detector leave straight tracks in the latter owing to a lack of magnetic field in the apparatus vicinity. However, multiple scattering in the heavy material of the detector can cause deviations of the muon trajectory. Its effect on the track angle and particle energy loss is discussed next in Section 6.1. Two complementary tracking methods used in the SND@LHC experiment are discussed in Section 6.2.

6.1 Tracking environment

Interactions in the heavy material between the electronic detectors planes are a challenge for particle tracking in the SND@LHC detector. These can be destructive processes that lead to muon absorption somewhere inside the detector and consequently inability to find a track. In other cases, processes like muon bremsstrahlung, delta-ray emission, and pair production generate additional activity in the detector and give rise to detector hits. Depending on the muon energy loss in these processes the number and energy of produced particles can be significant. However, this muon-induced radiation is typically colinear with the muon path and the corresponding hits are close to the muon ones. Further, there is also multiple scattering in the tungsten and iron. For low-energy muons, it can strongly deviate the muon trajectory, making it too bent to be fit. This is depicted in Figure 10, where the low-energy muon is in the end absorbed in the detector.

To demonstrate the effect of heavy material along the path of a high-energy particle, in Figure 11 the number of detector measurements per event are presented for data run 4705 and the passing-through-muons Monte Carlo simulation set dated March 2023. Detector measurements are either hits or clusters. The latter is a collection of fired adjacent detector elements. The time of a cluster is given by the earliest timestamp of any hit contributing to it. The data and simulation hit and cluster multiplicities do exceed the number of detector planes. For example, there are a total of 10 SciFi planes, 5 horizontal and 5 vertical, but the number of SciFi hits per event can be much larger than 10 for both data and passing-through-muons MC simulation. In each plot of Figure 11, the peak corresponds to a detector signal triggered by a passing-through muon. In Figure 11c, the larger value of the mean for data is explained by a displacement between the DS 1 horizontal bars and their readout SiPMs that appeared with time during the 2022 data-taking, see Figure 11e. Due to that shift, when a muon went through one bar, photons produced in that bar were collected by two SiPMs. Consequently, two digitized detector hits were created instead of a single one. The bar-readout shift appeared because the DS bars are manufactured with slightly different sizes and over time, gravity pulled them down with respect to SiPMs. To address this issue, special separators were installed between DS bars during the technical stop in the beginning of 2023. In general, data and MC simulation do show good agreement considering the number of hits and clusters per event.

The impact of heavy material along the muon trajectory in the detector can also be quantified in terms of energy loss, scattering angle, and displacement angles. The scattering angle, θ_{scatt}, is defined by the dot product of muon momenta entering (p_{in}) and going out (p_{out}) of a given volume:

$$\theta_{\text{scatt}} = \frac{(\overrightarrow{p_{\text{in}}} \cdot \overrightarrow{p_{\text{out}}})}{\text{p}_{\text{in}}\,\text{p}_{\text{out}}}. \tag{2}$$

The displacement angle is defined per projection, ($\theta_{\text{displ}_{\text{xz}}}$) and ($\theta_{\text{displ}_{\text{yz}}}$), as the ratio of the differences between X (or Y) and Z coordinates of a particle entering (x_{in}, y_{in}, z_{in}) and escaping (x_{out}, y_{out}, z_{out}) a given volume, i.e.

$$\theta_{\text{displ}_{xz}} = atan\left(\frac{\Delta x}{\Delta z}\right) = atan\left(\frac{x_{\text{out}} - x_{\text{in}}}{z_{\text{out}} - z_{\text{in}}}\right) \tag{3.1}$$

and

$$\theta_{\text{displ}_{yz}} = atan\left(\frac{\Delta y}{\Delta z}\right) = atan\left(\frac{y_{\text{out}} - y_{\text{in}}}{z_{\text{out}} - z_{\text{in}}}\right). \tag{3.2}$$

The energy loss, scattering, and displacement angles and their dependence on energy are plotted on Figures 12-14. Geant4 particle hit information in the detector is used. The four different regions under consideration are shown in Figure 12c. As shown in Figure 12a, muons at the scoring plane 60 m upstream of the detector that have energy less than a few tens of GeV, do not reach the detector. The median of energy losses in both the target and the DS region is about 1 GeV. The energy

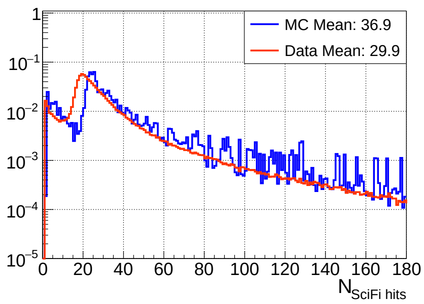

(a)

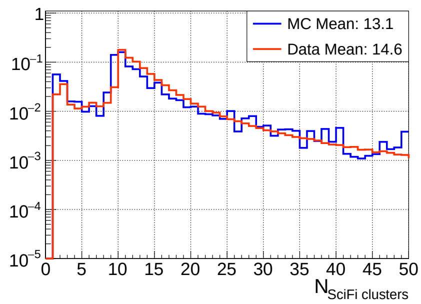

(b)

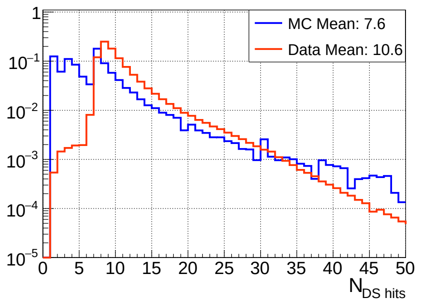

(c)

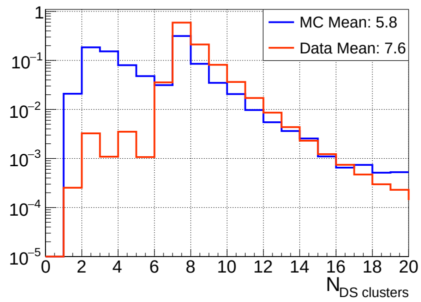

(d)

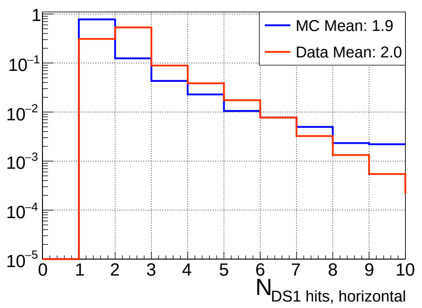

(e)

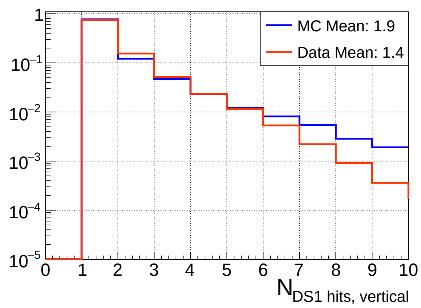

(f)

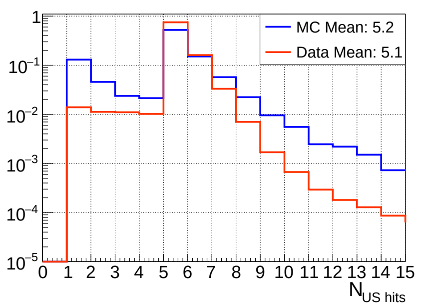

(g)

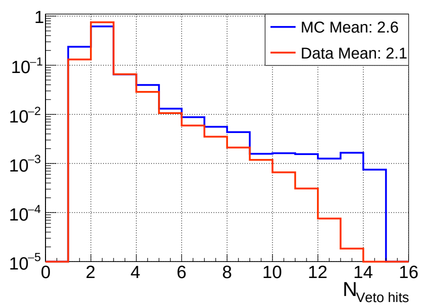

(h)

Figure 11: Detector measurement multiplicity per event for data (red) and Monte Carlo simulation (blue): SciFi hits (a) and clusters (b), DS hits (c) and clusters (d), DS1 hits in horizontal (e) and in vertical (f) bars, US hits (g), and Veto hits (h). They are all normalized to unit integral. The mean of each distribution is reported in the legend.

loss in the DS system for some muons is much lower than that. It is confirmed that these are muons passing through the very upper parts of the DS stations, which are not covered by the slightly shorter iron blocks. Thus energy loss for these particles is much lower.

The muon energy loss and scattering angle as functions of the initial muon energy before entering the target or the DS regions are shown in Figure 13. There is a wide spread in the energy losses for muons of energies above 200 GeV. Most muons, however, have lower energies and the respective losses are around 1 GeV, reported also in Figure 12a. As for the angles, low-energy muons can undergo large-angle scattering, while for muons above 30 GeV energy, the scattering is restricted to a 10 mrad angle in both the target and the DS regions.

Another angular parameter is the displacement angle, see Equation 3. The distribution vs energy of the XZ and the YZ displacement angles in the target and the DS are plotted on Figure 14. A secondary angular direction, in the horizontal plane, is visible in Figures 14a and 14c. It does not correspond to a specific muon source, but rather to muon production via particle decay or interactions in various machine elements on the path from IP1. The muons angular distribution at the SND@LHC detector is discussed in more detail in Section 7.

6.2 Tracking methods

Two tracking methods were developed in the SND@LHC analysis framework. They differ in the way to find track candidates. One of the tracking methods makes use of a custom track finding solution. It is dubbed simple tracking(ST). The other tracking approach employs the Hough transform [18, 19] pattern recognition method and is referred to as Hough Transform(HT). In both cases, the track fitting is done using the Kalman Filter [20, 21] method in the GENFIT package [22, 23]. Each system's resolution for a single plane measurement, see Section 2.1, is used to set the covariance matrix elements used by the Kalman Filter.

Since all SciFi planes and vertical DS planes are read out on one side, their hits have two well defined spatial coordinates. Then, tracking in these syb-systems is done separately in the horizontal $x - z$ and vertical $y - z$ plane. The final 3D track is built combining the two 2D tracks. Events with multiple track candidates per projection can be reconstructed, but it creates degeneracy as to which two projections belong to the same 3D particle trajectory. These multi-track cases are treated differently by the two tracking algorithms.

6.2.1 Simple tracking

The simple tracking is used for the detector alignment and online monitoring during data-taking. The specific properties of the ST are

- track building blocks are clusters of detector hits,
- tracking is only performed if at least 3 horizontal and also 3 vertical detector planes have no more than 5 clusters,

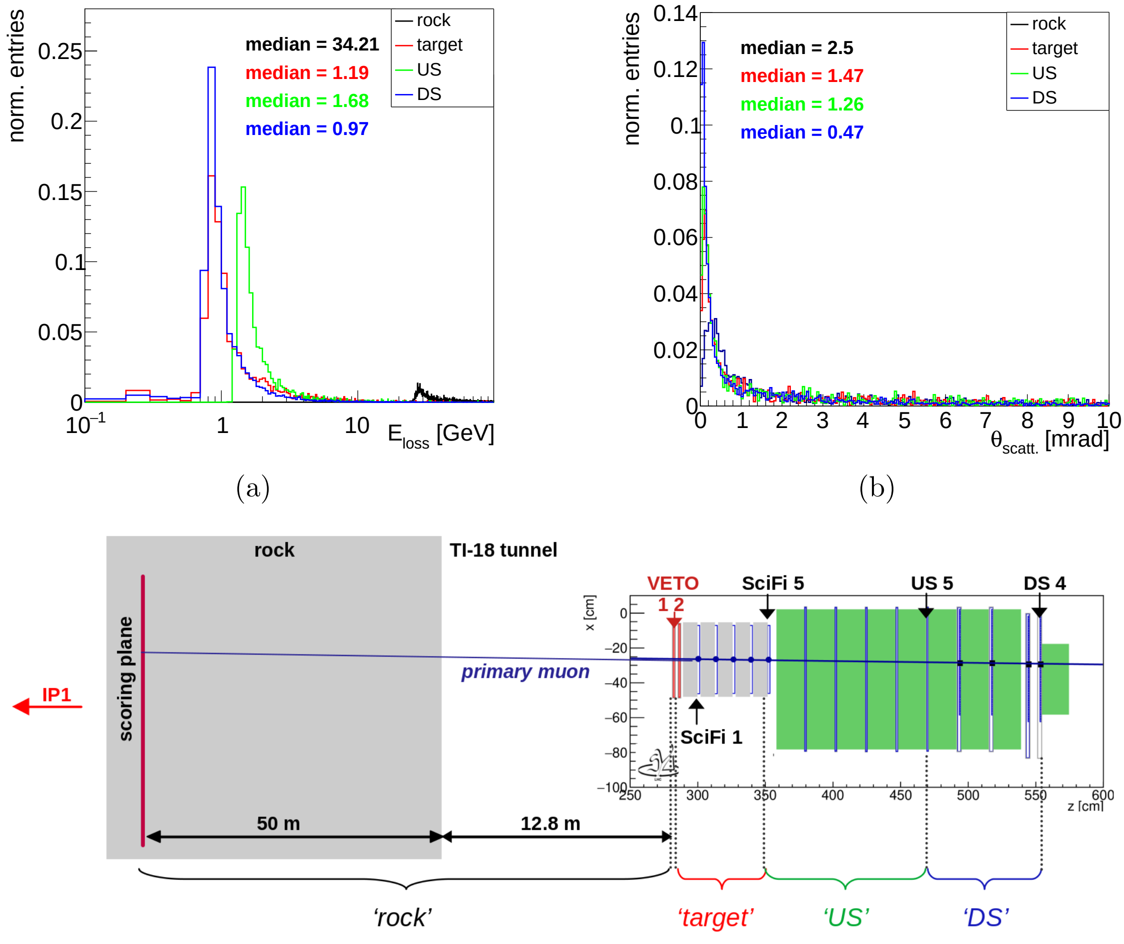

(a) (b)

(c)

Figure 12: Energy loss (a) and scattering angle (b) for muons passing through different volumes (c) between the scoring plane and the detector. The distributions are normalized to unit integral. The distance between the scoring plane and the detector is not to scale. There are 50 meters of rock and 12.8 meters of air between the scoring plane and the SND@LHC apparatus. The region between the scoring plane and the very first detector element, Veto 1, is denoted as 'rock'. The label 'target' is for the neutrino target, i.e. the tungsten plates. However, the target here includes all materials between Veto 2 and SciFi 5. The US region starts at SciFi 5 and ends at the last US 5 station. The DS region spans from US 5 to the last DS 4 station.

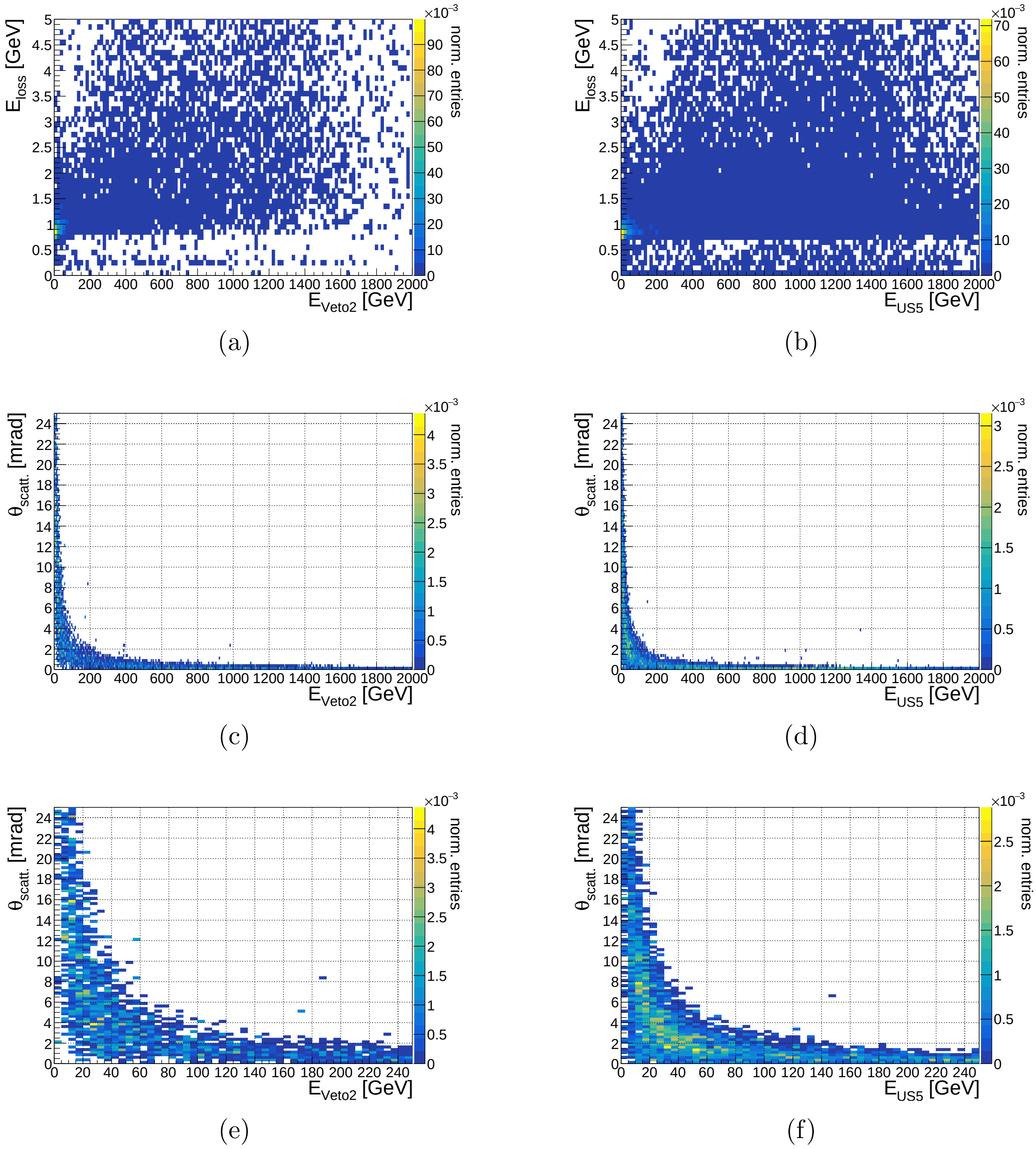

Figure 13: Energy loss vs E (a, b) and scattering angle vs E (c, d), also magnified in (e, f), for muons passing through the target(left side) and the DS regions(right side). The schematic drawing in Figure 12c depicts the target and the DS areas. The in-going energy of the muon entering each region is plotted on the abscissa.

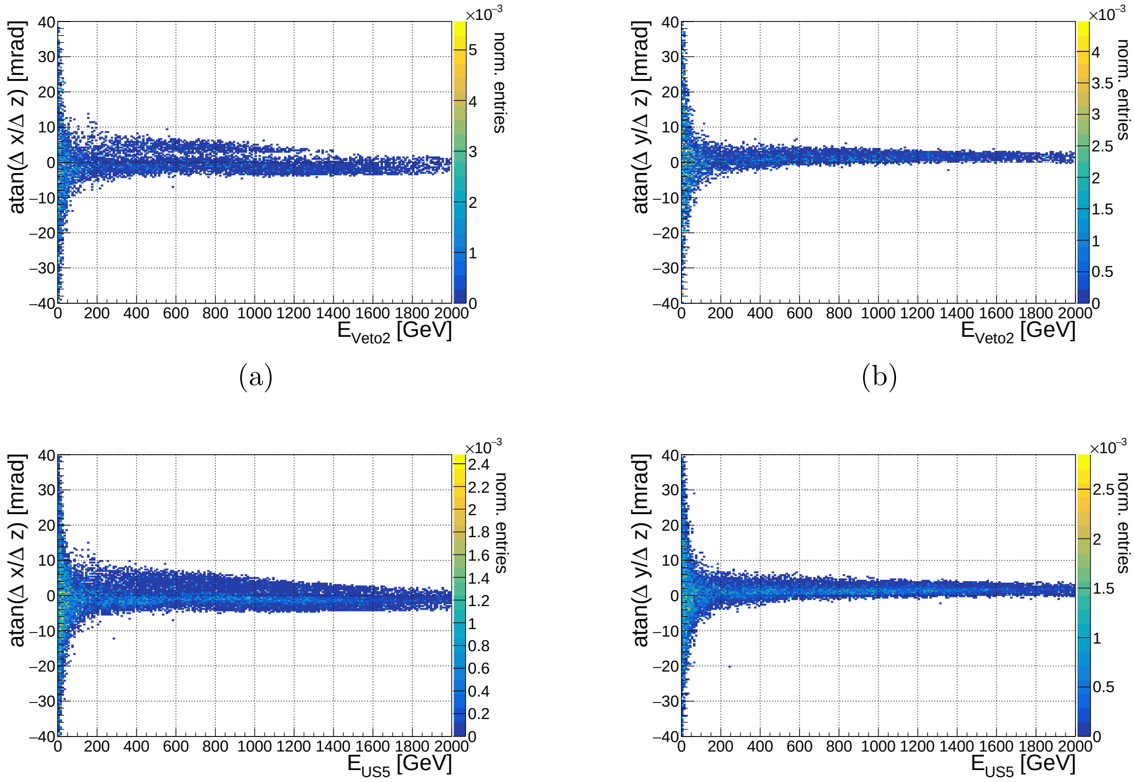

(a) (b)

(c) (d)

Figure 14: Displacement angles in the target (a, b) and the DS (c, d) in XZ(left panels) and YZ(right panels) projections. The schematic drawing in Figure 12c depicts the target and the DS areas. The in-going energy of the muon entering each region is plotted on the abscissa.

- to attempt DS tracking:
  - at least one plane has to have a single cluster, denoted a *seed cluster*
  - two planes together cannot have more than 6 clusters
- for SciFi tracking:
  - the SciFi planes with the highest occupancy are not used in the tracking (to avoid spurious associations) as long as there are at least 3 planes to allow a track fit
- the track fit is a straight line fit.

The SciFi track finding algorithm makes a straight-line fit in each projection and provides a list of clusters to the track fitter. While this track finding procedure is best suited to having one cluster per plane and projection, it also performs well with additional noise measurements. For the latter case, a coarse rejection of outlier clusters is made. Measurements having a cluster-to-fit residual larger than 7.5 mm are removed. The cut value is determined by scanning event displays. For reference, typical SciFi residuals are below 200 µm, as shown in Figure 5.

The DS track finding is based on minimization of the track residual. To start, lines are built for each combination of the seed cluster with clusters in the other planes that have the second lowest cluster occupancy, the plane of the seed cluster being the least occupied. Then, each line prediction is extrapolated to the remaining planes and the distance to clusters is calculated. The cluster combination with the smallest residual is chosen.

It is possible to reconstruct multiple SciFi tracks in an event using simple tracking. The successful track candidates must have spatially well separated clusters, on the level of a few centimeters, in different tracking stations. This capability allows to study multi-trajectory events. However, it is not used to asses the muon rate in the detector.

6.2.2 Hough transform

The other tracking alternative, the Hough transform, has been developed to allow tracking in busy environments. Initially, the procedure was tuned to find muons produced in muon neutrino charged-current(CC) interactions. In the muon neutrino CC events, alongside the outgoing muon, a hadronic shower develops and generates numerous hits in the detector elements. Events with high hit occupancy may also originate from the passage of muons from the IP. Muons can interact in the detector material and produce multiple particles, mainly delta electrons and gamma rays. If the energy of these products is large enough, they initiate electromagnetic showers, which may span over one or more tracking stations. In both penetrating muons and neutrino CC interaction events, disentangling the muon from the accompanying shower is made possible using the powerful Hough transform method. Its role is to detect a line in the complicated picture of numerous fired detectors per tracking plane.

For the HT, when there are more than one track candidates per projection, it is checked whether the found candidates have a compact sample of slopes, i.e. that the predicted slopes are contained in a range comparable to the detector angular resolution. If that is the case, then the candidate having the slope closest to the sample's median is selected. In all other cases, the track fit is dropped. This strategy is well suited for the passing-through muon case. However, the HT procedure is also capable of finding multiple tracks per event.

After a track candidate has been found, it is verified to have passed through fired detector elements within a tolerance level. Much like the ST case, the requirement is that the HT line crosses within the tolerance at least 3 horizontal and 3 vertical planes. After that, the coordinates of these hit detector elements are used by GENFIT's Kalman Filter for a final 3D track fit. In more numerical details, the specific points for the Hough transform tracking are

- track building blocks are detector hits,
- tracking is only performed if at least 3 horizontal and 3 vertical detector planes (SciFi) or stations (DS) have hits,
- events with multiple 2D track projection candidates are treated as follows: if predicted slopes are contained in a range comparable to the detector angular resolution, the track with the slope closest to the sample's median is chosen. Otherwise, the event is dropped.
- at least 3 horizontal and 3 vertical tracking planes have hit detector elements that are crossed by the predicted track. It is checked that the line passes through fired detector elements within a tolerance level. The tolerance is 0.1 cm for SciFi and 1 cm for DS tracking case. The SciFi tolerance value is equivalent to the distance between 4 SciFi SiPM channels. For the DS tracking, the tolerance level is equal to the DS bar transverse size.
- in low-hit-occupancy events, namely when detector planes have less than 4 hits each, the tolerance levels are increased to 0.5 cm for SciFi and 3 cm for DS. The aim is to maximize tracking efficiency while keeping the risk of building ghost tracks low.
- for SciFi tracking, when detector planes have less than 3 hits each, the user-defined precision of the Hough transform method is scaled down. It allows to find a track candidate using fewer measurements, which sometimes do not lie on a perfectly straight line due to multiple scattering. This tune is implemented to improve the tracking efficiency for low-energy muons, see Section 6.3.

6.2.3 A final remark on tracking methods

A notable difference between simple tracking and the Hough transform is that the first one uses detector clusters, while the second uses detector hits. Both measurement objects have their advantages. In SciFi for example, one SiPM channel can

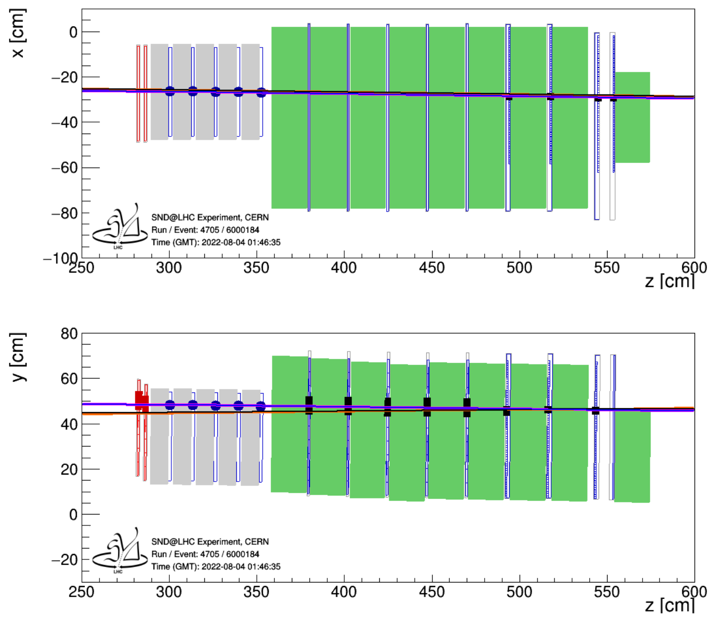

Figure 15: A SND@LHC 2D event display of a data event where SciFi and DS tracks using ST and HT are successfully built. SciFi tracks are drawn as blue and magenta lines for ST and HT, respectively. DS tracks are colored in black for ST and in orange for HT. The top panel shows the horizontal XZ plane, while the bottom one shows the vertical YZ plane. ST and HT SciFi tracks are well aligned on top of one another. Similarly, the ST and HT DS tracks are practically indistinguishable on the display. Due to the larger DS track angle resolution, the DS track extrapolation over large distances can lead to few-centimeter mismatches, e.g. between SciFi and DS tracks at same Z planes in SciFi. Detector hits in the Veto, the SciFi, and the hadronic calorimeter are shown as red bars, blue markers and black bars, respectively.

collect photons from multiple fibers. Hence, clustering SciFi hits seems imposed by detector construction. On the other hand, as there is substantial material budget between tracking planes, it is likely that various particles, electrons, gamma rays, etc., induce signals in neighbouring SiPM channels. Clustering would then combine all these together, compromising the origin of the measurement. Taking these two points into account, the Hough transform, which has the power to distinguish between separate SiPM channels, uses detector hits. Alternatively, the performance of the simple tracking is boosted by reducing the number of track building points using clusters.

We close the tracking overview with an event display in Figure 15 of a clean SND@LHC event, where SciFi and DS tracks using ST and HT are successfully built.

6.3 MC tracking efficiency

The MC tracking efficiency of the ST and the HT procedures are assessed using the passing-through muons simulations described in Section 4. The MC tracking efficiency is defined as

$$\epsilon^{MC} = \frac{\text{Number of events with a reconstructed muon track}}{\text{Number of simulated events with a reconstructible muon track}}. \quad (4)$$

In the denominator, a reconstructible track is the track of a particle leaving at least 3 MC points in horizontal and 3 MC points in vertical detector elements. The latter takes into account that three measurements per projection are required to attempt any of the two tracking methods.

The MC tracking efficiencies per SciFi and DS systems using the two tracking procedures are reported in Table 3. To better understand the differences in the observed values, in Figures 16-17 the MC tracking efficiency is plotted as a function of two parameters - number of detector measurements, and muon energy at its entry point into the detector. For SciFi simple tracking, the tracking efficiency is stable for events where the cluster multiplicity is not too large, i.e. below 20. Then, the efficiency falls when increasing the number of clusters per event. The reason is that events with high detector activity fail the criterion on number of clusters per plane and track fits are not attempted. The same rationale explains the efficiency's gradual decrease with increasing muon energy. For high-energy muons, particle production via bremsstrahlung, delta rays, or pair production is enhanced and cluster multiplicity per plane increases, lowering down track fit trials. To a much lesser extend the same trends are exhibited for DS simple tracking. However, the MC tracking efficiency for the DS ST is high in any bin.

Much like the DS simple tracking case, the DS Hough transform tracking efficiency is about 98 % and stable in the whole muon energy and hit multiplicity range. On the other hand, the SciFi Hough tracking efficiency is lower for less hit-busy events compared to those having large hits counts. In terms of muon energy, there is a pronounced dip in efficiency for low-energy muons, when their energy is below 20 GeV. These two observations combined mean that about 20% of low-energy muons that penetrate through at least 3 detector planes undergo large-angle multiple scattering inside the target region. In such cases, the straight-line Hough transform prediction fails to go through sufficient number of planes to pass the tracking criteria. Inspection of such events further shows that sometimes these low-energy muons are absorbed in the tungsten plates between SciFi tracking stations. For more information on multiple scattering in the detector, refer to Section 6.1.

6.4 Tracking efficiency with data

Another way to assess the tracking efficiency is to use the independent track builds from SciFi and DS systems. The strategy is to use SciFi tracks as a tag to estimate DS tracking efficiency and vice versa. The main benefit of this approach is the large available data statistics well covering the full detector acceptance. Even so, due to the smaller size of the SciFi detector compared to the DS system and the

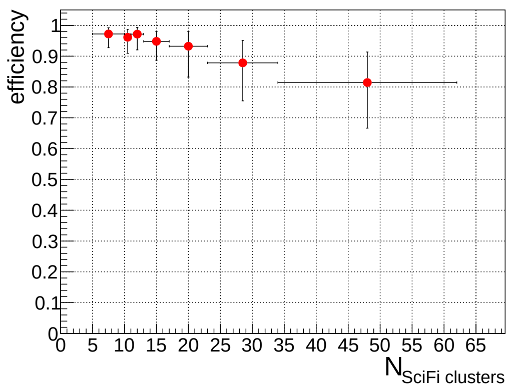

(a)

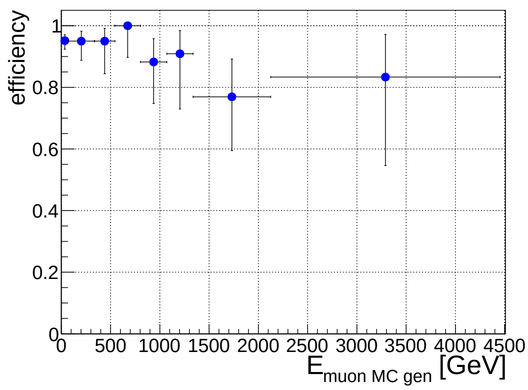

(b)

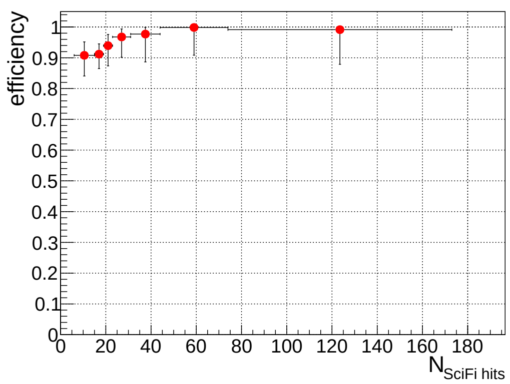

(c)

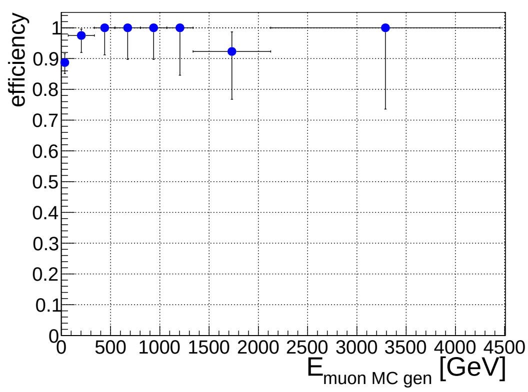

(d)

Figure 16: SciFi Monte Carlo tracking efficiency vs number of measurements (a and c) and vs generated muon energy (b and d) for tracks built using simple(top) and Hough transform(bottom) tracking procedures. The efficiency definition is given in Equation 4. The Clopper-Pearson statistics option and a 90 % confidence level are used to compute the confidence intervals.

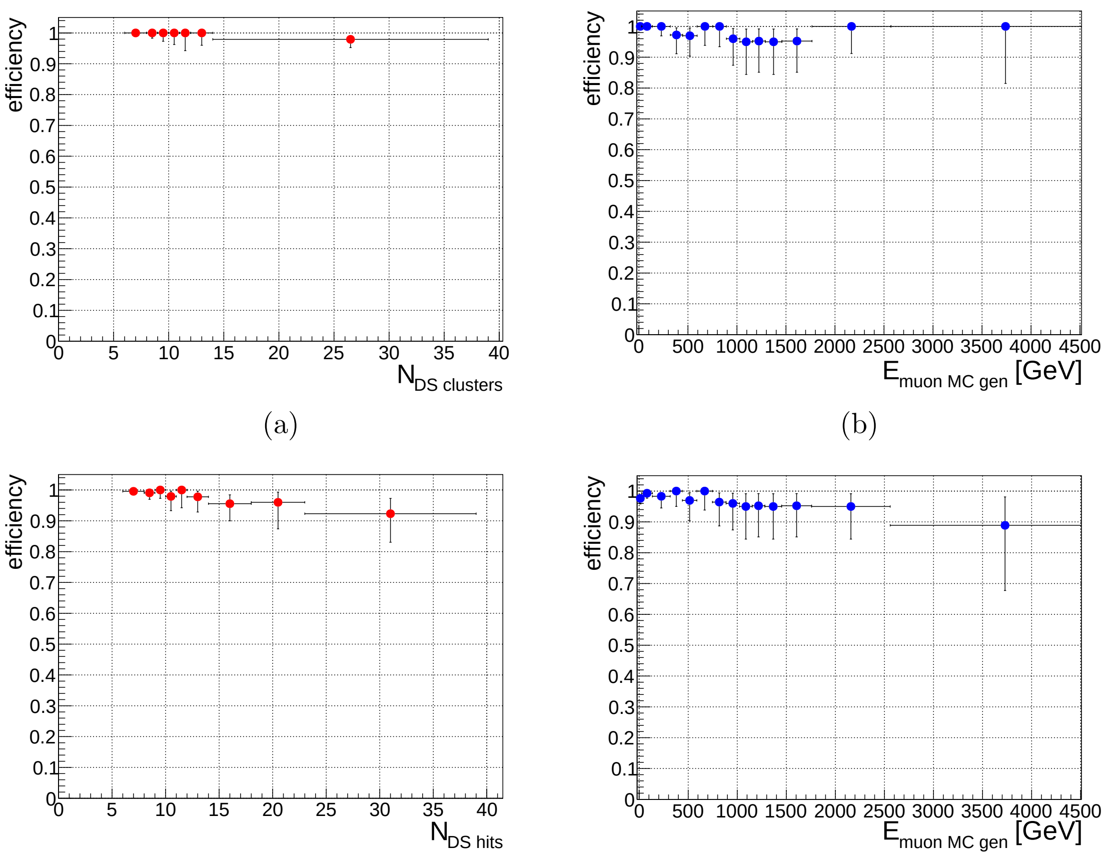

(a) (b) (c) (d)

Figure 17: DS Monte Carlo tracking efficiency vs number of measurements (a and c) and vs generated muon energy (b and d) for tracks built using simple(top) and Hough transform(bottom) tracking procedures. The efficiency definition is given in Equation 4. The Clopper-Pearson statistics option and a 90 % confidence level are used to compute the confidence intervals.

system	tracking algorithm	MC tracking efficiency
SciFi	simple tracking	0.93 ± 0.03
	Hough transform	0.94 ± 0.03
DS	simple tracking	0.98 ± 0.02
	Hough transform	0.98 ± 0.02

Table 3: Monte Carlo tracking efficiency using the SciFi and DS detectors and applying simple and Hough transform tracking procedures. The efficiency definition is given in Equation 4. Statistical uncertainties are reported.

positions of the main muon sources with respect to the detector, only a part of the DS acceptance can be probed with this method. Nonetheless, it is assumed the obtained DS tracking efficiency can be applied to the full detector fiducial volume. Reasons for it are given in Section 6.4.2.

Another benefit of the data-based tracking efficiency is that the intrinsic spatial and energy distributions of muons at the detector are used. Since the energy loss and number of hits produced in the apparatus vary with muon energy, see Section 6.1, the data provides the best conditions to test the tracking methods. Additionally, using data to define tracking efficiency means there is no need to rely on external detector area description, as is the case for simulations. Materials and their positions along the particle's path, with the exception that the detector has to be spatially aligned, are identical for all data measurements. Lastly, any particle registration inefficiency, due to dead zones inside tracking planes or detector readout inefficiency (dead time, saturation, or else) are by construction included in the data-based tracking efficiency.

6.4.1 SciFi tracking efficiency using data

The data SciFi tracking efficiency procedure is

- For each event, take a good DS track
  - converged fit, slopes in both projections below 80 mrad, $\chi^2/ndf < 5$.
- Check if the extrapolated DS track at the Veto planes is within 3 cm of a fired Veto bar. The tolerance value used here should not be too large, otherwise DS tracks outside of the Veto acceptance, and so of the SciFi one, will be selected.
- Extrapolate the DS track to a reference plane at $z = 490$ cm and fill a 2D XY histogram with DS track intersection coordinates. The reference plane is located at the position of the first DS station. It is done to minimize extrapolation of DS tracks since they have worse angular resolution compared to SciFi tracks.
- take a good SciFi track in the same event,
  - converged fit, $\chi^2/ndf < 20$.
- Extrapolate the SciFi track to the same reference plane,

- If SciFi track's and DS track's projections on the reference plane are within 3 cm distance, fill a 2D XY histogram with DS track intersection,
- The ratio of the two histograms is an estimate of the SciFi tracking efficiency using data.

The choice of selection parameters is motivated in Figures 18 and 19, where data and Monte Carlo simulation distributions of χ^2/ndf and the distances between extrapolated tracks and detector elements are shown. The selection cut for DS tracks at Veto planes is determined by the half size of the Veto bar, since it is the bar center that is used in the calculation.

The 2D XY histogram of the SciFi tracking efficiency using data is presented in Figure 20 for simple tracking and in Figure 21 for Hough transform tracks. Only the central region of the detector, where the efficiency is relatively uniform in $x-y$ space, is used to obtain the data tracking efficiency. The selected fiducial volume is $-42\,\text{cm} \le x \le -11\,\text{cm}$ and $18\,\text{cm} \le y \le 49\,\text{cm}$. It corresponds to a $31{\times}31\ \text{cm}^2$ detector area. The mean of all efficiency values in $x-y$ bins, their distributions presented in Figures 20b and 21b, is assigned as the final data tracking efficiency. The mean and standard deviation for both SciFi tracking alternatives are summarized in Table 4.

6.4.2 DS tracking efficiency using data

The outline of the data DS tracking efficiency method is

- For each event, take a good SciFi track
  - converged fit, slopes in both projections below 80 mrad, $\chi^2/ndf < 20$.
- Check if the extrapolated SciFi track at US 5 plane is within 3 cm of a fired US 5 bar,
- Check if the extrapolated SciFi track at DS 3 plane is inside its geometrical acceptance within a 3-cm tolerance,
- Extrapolate SciFi track to a reference plane at $z = 490$ cm and fill a 2D XY histogram with SciFi track intersection coordinates. The reference plane is located at the position of the first DS station.
- Take a DS track in the same event
  - converged fit, $\chi^2/ndf < 5$.
- Extrapolate it to the same reference plane,
- If DS track's and SciFi track's projections on the reference plane are within 3 cm distance, fill a 2D XY histogram with SciFi track intersection,
- The ratio of the two histograms is an estimate of the DS tracking efficiency using data.

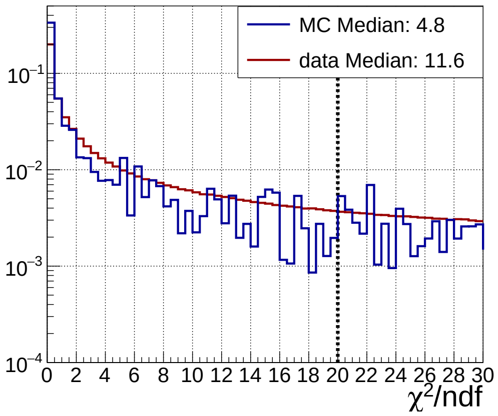

(a)

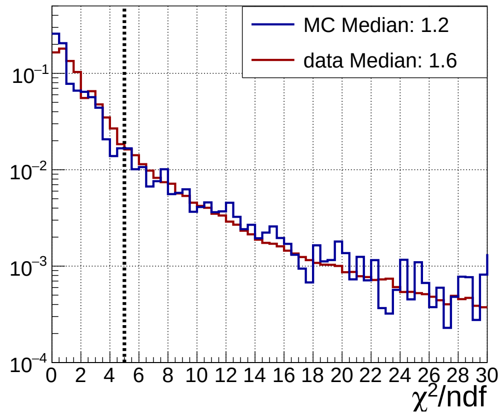

(b)

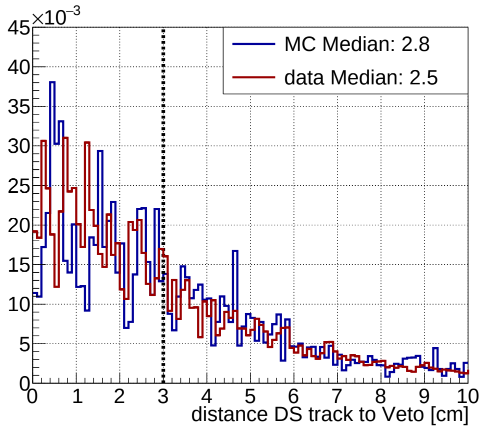

(c)

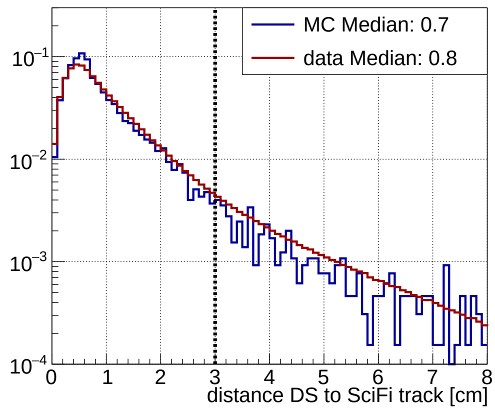

(d)

Figure 18: χ^2/ndf for SciFi (a) and DS (b) tracks built using the simple tracking, distance between ST DS track and a fired Veto bar (c), and distance between a ST SciFi track and a ST DS track extrapolated position to a reference plane at $z = 490$ cm (d). The cut values used in the SciFi tracking data-based efficiency estimation are noted with a dotted black line. They correspond to 2-3 times the median, i.e., 0.5 quantile, of the data distributions.

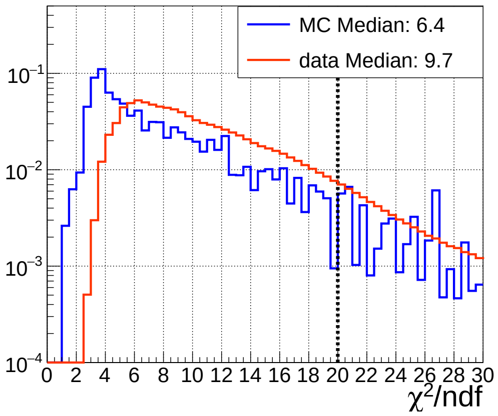

(a)

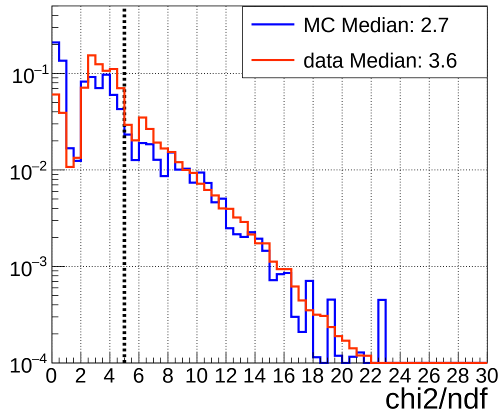

(b)

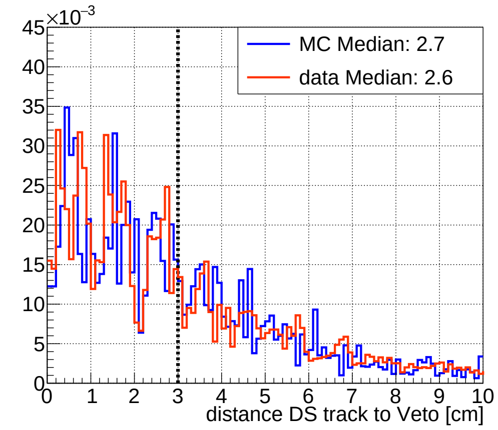

(c)

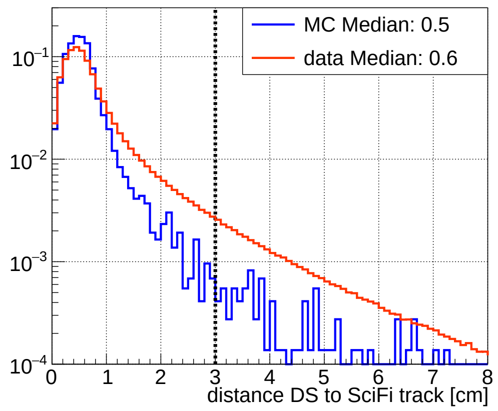

(d)

Figure 19: χ^2/ndf for SciFi (a) and DS (b) tracks build using the Hough transform, distance between HT DS track and a fired Veto bar (c), and distance between a HT SciFi track and a HT DS track extrapolated position to a reference plane at $z = 490$ cm (d). The cut values used in the SciFi tracking data-based efficiency estimation are noted with a dotted black line. They correspond to 2-3 times the median, i.e., 0.5 quantile, of the data distributions.

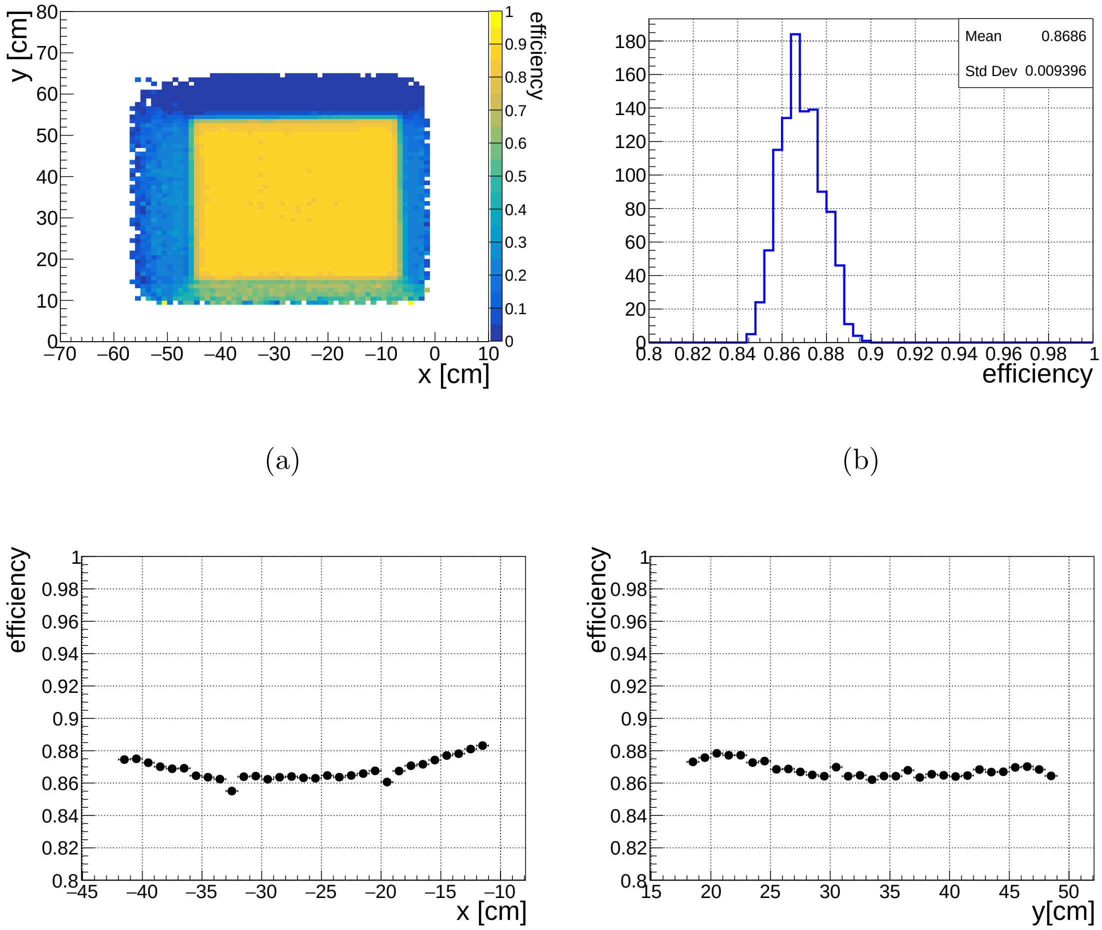

(a) (b) (c) (d)

Figure 20: SciFi simple tracking efficiency obtained using the data. ST DS tracks are used as tags. The efficiency in $x-y$ bins (a) is used to determine a central region of relatively uniform efficiency. The fiducial volume selected is $-42\,\text{cm} \leq x \leq -11\,\text{cm}$ and $18\,\text{cm} \leq y \leq 49\,\text{cm}$. In that range the efficiency vs x (c) and y (d) position fluctuates by a few percent. The Clopper-Pearson statistics option and a 90 % confidence level are used to compute the confidence intervals for the efficiency in x (c) and y (d) bins. The final efficiency value is the mean over $x-y$ bins in the selected fiducial volume, shown on plot (b).

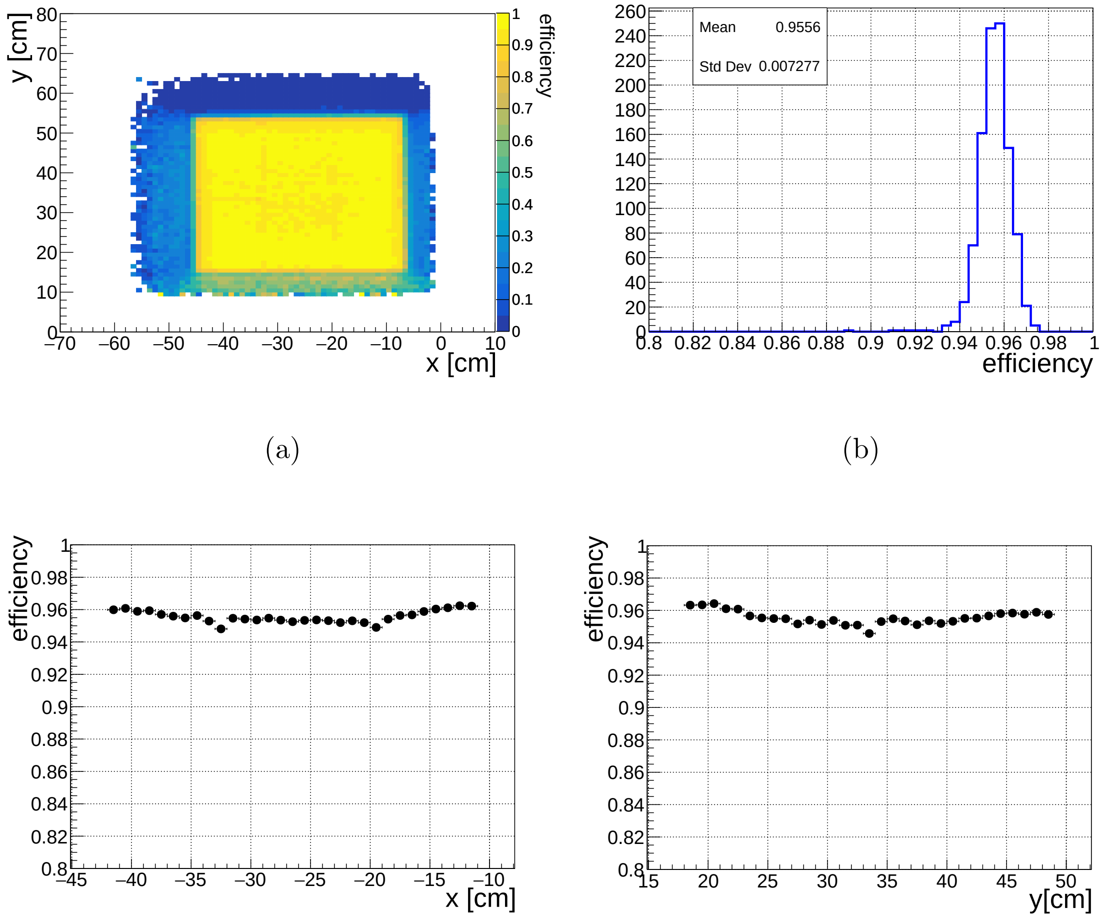

(a) (b)

(c) (d)

Figure 21: SciFi Hough transform tracking efficiency obtained using the data. HT DS tracks are used as tags. The efficiency in $x - y$ bins (a) is used to determine a central region of relatively uniform efficiency. The selected fiducial volume is $-42\,\mathrm{cm} \leq x \leq -11\,\mathrm{cm}$ and $18\,\mathrm{cm} \leq y \leq 49\,\mathrm{cm}$. In that range, the efficiency vs x (c) and y (d) position fluctuates by a few percent. The Clopper-Pearson statistics option and a 90 % confidence level are used to compute the confidence intervals for the efficiency in x (c) and y (d) bins. The final efficiency value is the mean over $x - y$ bins in the selected fiducial volume, shown on plot (b).

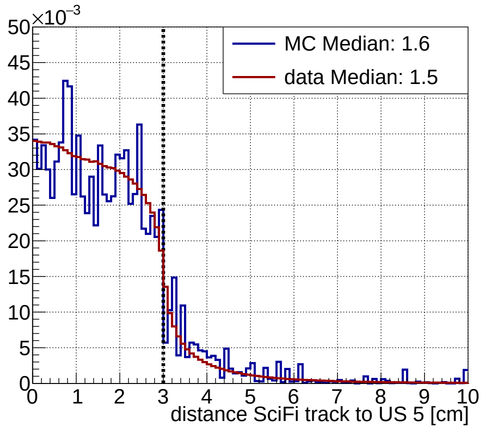

(a) (b)

Figure 22: The distance between a ST SciFi track and a fired US 5 bar (a), and distance between a HT SciFi track and a fired US 5 bar (b). The cut value at 3 cm that is used in the DS tracking data-based efficiency estimation is noted with a dotted black line.

The selection cut for SciFi tracks at US 5 planes is determined by the half size of a US bar, since it is the bar center that is used in the respective calculation. The data and Monte Carlo simulation distributions of the distance between a SciFi extrapolated track and fired US 5 bars are shown in Figure 22 for the simple and the Hough transform tracking cases.

The 2D XY histogram of data DS tracking efficiency is presented in Figure 23 for simple tracking and in Figure 24 for Hough transform tracks. Due to the difference in the SciFi and the DS dimensions, the DS acceptance is partially covered by extrapolated SciFi tracks. Consequently, the DS detector region of uniform efficiency, which is used to obtain the data tracking efficiency, is identical to the one reported in Section 6.4.1 for the SciFi tracking efficiency. Again, the selected fiducial volume is $-42\,\text{cm} \leq x \leq -11\,\text{cm}$ and $18\,\text{cm} \leq y \leq 49\,\text{cm}$. The mean of all efficiency values in $x-y$ bins, the latter presented in Figures 23b and 24b, is assigned as the final data DS tracking efficiency. The mean and standard deviation of the efficiency for all detectors and tracking methods are summarized in Table 4. They will be used to asses the systematic uncertainty of the muon flux in the detector.

The DS tracking efficiency in the selected spatial region fluctuates by a few percent with vertical position change, see Figures 23d and 24d. Looking at DS hit distributions per station and bar, it is confirmed the observed fluctuations originate from bar inefficiencies. There are 3 horizontal DS stations and all of them must have at least one hit to attempt a track fit. As there is no plane redundancy for the DS track fits in the vertical projection, the tracking efficiency is slightly lower in the areas of those inefficient bars. Since the observed non-uniform behaviour of the DS tracking efficiency obtained using the data is understood, it is considered that the efficiency estimate can be safely applied to the full acceptance of the DS system.

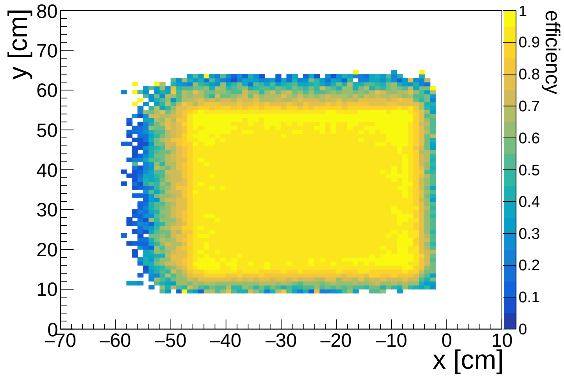

(a)

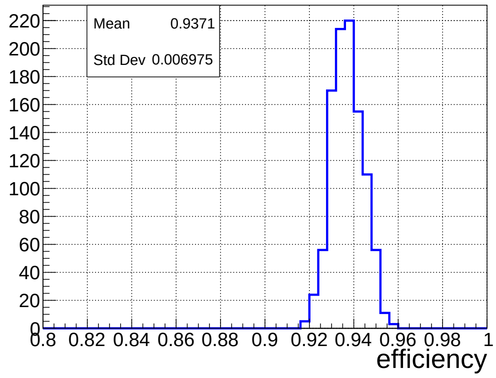

(b)

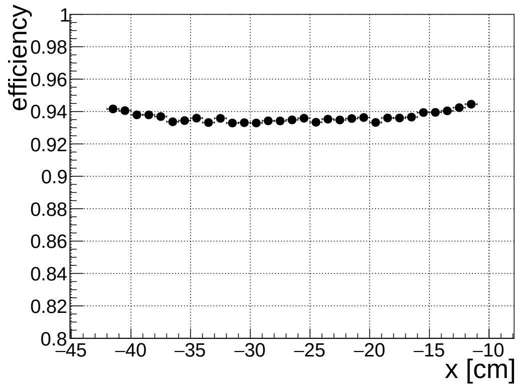

(c)

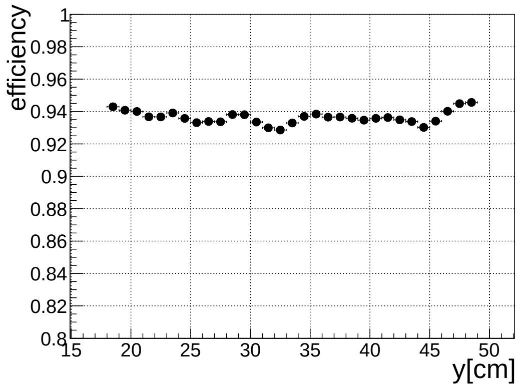

(d)

Figure 23: DS simple tracking efficiency obtained using the data. ST SciFi tracks are used as tags. The efficiency in $x-y$ bins (a) is used to determine a central region of relatively uniform efficiency. The fiducial volume selected is $-42\,\mathrm{cm} \leq x \leq -11\,\mathrm{cm}$ and $18\,\mathrm{cm} \leq y \leq 49\,\mathrm{cm}$. In that range, the efficiency vs x (c) and y (d) position fluctuates by a few percent. The Clopper-Pearson statistics option and a 90 % confidence level are used to compute the confidence intervals for the efficiency in x (c) and y (d) bins. The final efficiency value is the mean over $x-y$ bins in the selected fiducial volume, shown in plot (b).

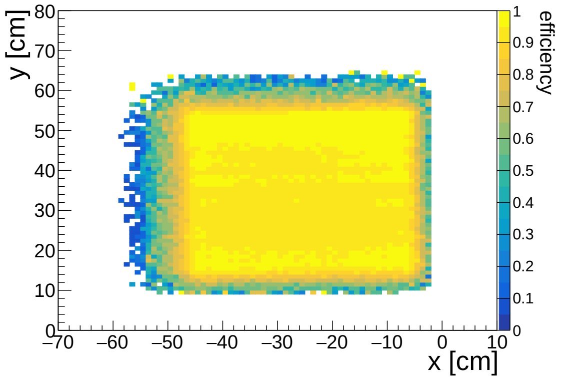

(a)

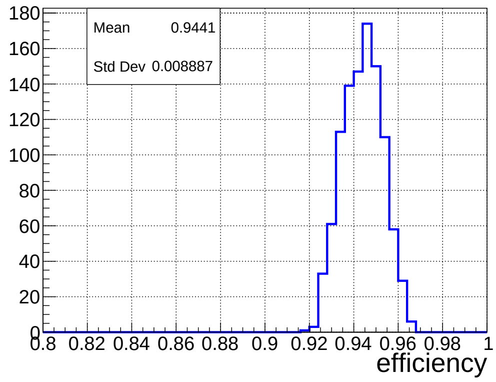

(b)

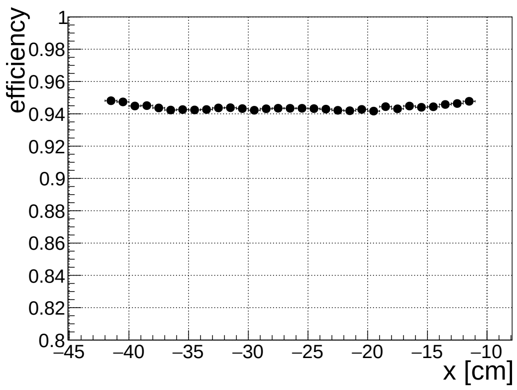

(c)

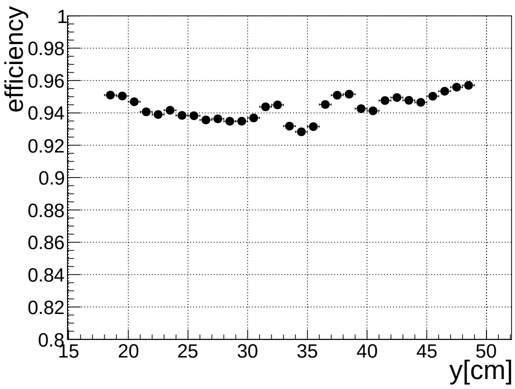

(d)

Figure 24: DS Hough transform tracking efficiency obtained using the data. HT SciFi tracks are used as tags. The efficiency in $x - y$ bins (a) is used to determine a central region of relatively uniform efficiency. The selected fiducial volume is $-42\,\text{cm} \leq x \leq -11\,\text{cm}$ and $18\,\text{cm} \leq y \leq 49\,\text{cm}$. In that range, the efficiency vs x (c) and y (d) position fluctuates by a few percent. The Clopper-Pearson statistics option and a 90 % confidence level are used to compute the confidence intervals for the efficiency in x (c) and y (d) bins. The final efficiency value is the mean over $x - y$ bins in the selected fiducial volume, shown in plot (b).

system	tracking algorithm	Data tracking efficiency
SciFi	simple tracking	0.868 ± 0.009
	Hough transform	0.956 ± 0.007
DS	simple tracking	0.937 ± 0.007
	Hough transform	0.944 ± 0.009

Table 4: Tracking efficiency using the data. Reported results are for SciFi and DS detectors, applying simple and Hough transform tracking procedures. The quoted values are mean and standard deviation over binned efficiencies in $x-y$ coordinates.

7 Angular distribution

Due to the position of the SND@LHC detector 480 m away from IP1 and at a small off-axis angle, one expects that surviving long-range muons leave traces in the detector that are at small angles with respect to the SND@LHC's Z axis. This is exactly the case shown in Figure 25. The central peak corresponds to a distant source at IP1. This peak has large tails due to multiple scattering along the 480-m path from IP1 to the TI-18 tunnel.

In the logarithmic scale of track slopes in the $x-z$ plane, see Figures 25c and 25d, a few structures at negative slopes become visible. The origin of particles passing through the detector at such angles is beam-gas interactions in the beamline. As shown in Figure 26, after selecting events in sync with LHC bunches corresponding to non-colliding Beam 2 - no Beam 1 (B2noB1), the vast majority of reconstructed tracks have negative XZ slopes. Moreover, track direction studies based on detector hit timing show that tracks in Beam 2 events enter the detector from the back, see Figure 27. Then, the origin of these particles is downstream of the DS stations. The reconstructed angles point to elements in the LHC half-cells 12-17, with angles approaching 0 for more distant sources. For reference, a schematic view of the relevant part of the LHC complex, taken from the CERN GIS portal [24] is given on Figure 28.

A closer look at the central region of the main peak in Figure 29 shows two slightly shifted sub-peaks. The angular distance in the $x-z$ plane between these sub-maxima is about 5 mrad. An identical two-peak structure is observed in the emulsion data too. As reported in Reference [8], the difference in slope between the two peaks in the emulsion data is also 5 mrad and matches the electronic detectors measurement. Similarly to the main-peak case, muons contributing to the smaller central sub-peak originate from interactions and particle (pion and kaon) decays at various locations. Among the more interesting cases, a contribution comes from interactions in the area where the clock-wise circulating LHC proton beam starts to be bent in the LHC circular orbit. That is approximately the quadrupole magnet of half-cell 9 and is 345 m away from IP1. For clarity, this is shown on the map in Figure 30. Another case are interactions in the area where the nominal IP1 collision axis intersects the ground outside the curved LHC tunnel in the direction of the TI-18 tunnel. This information is deduced thanks to FLUKA simulations, whose output purposefully provides the production history of muons reaching the scoring

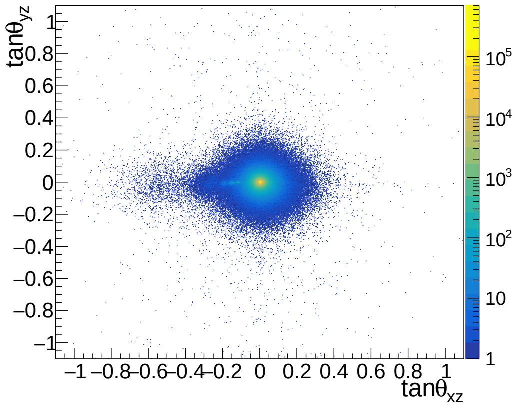

(a)

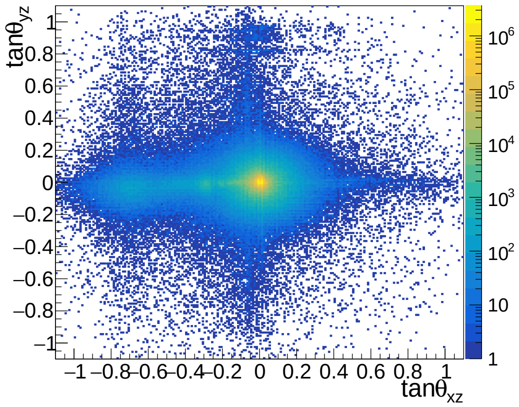

(b)

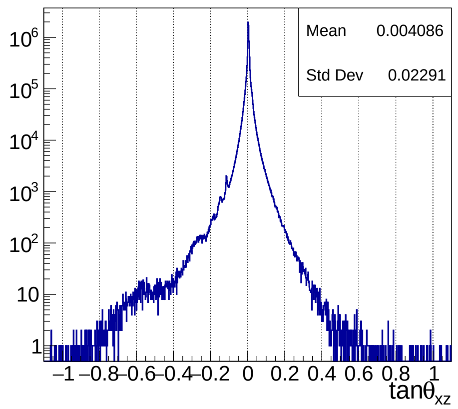

(c)

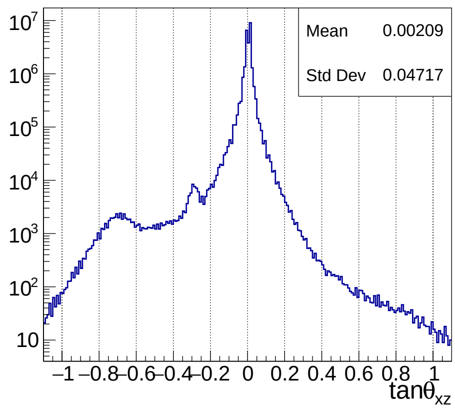

(d)

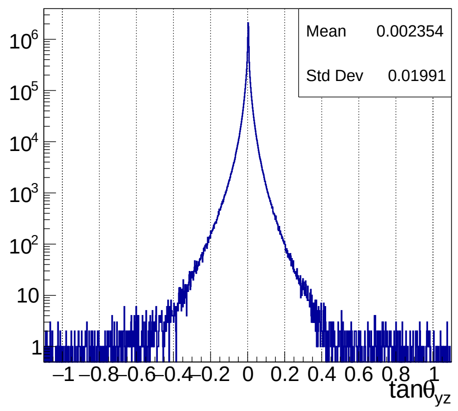

(e)

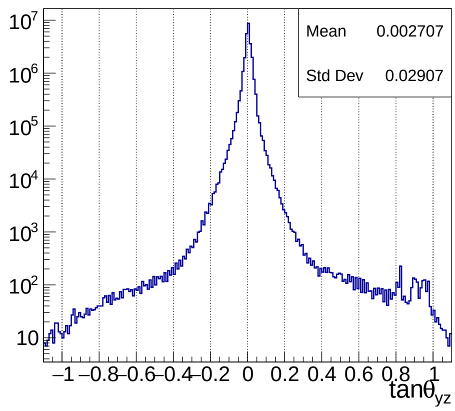

(f)

Figure 25: SciFi (a, c, e) and DS (b, d, f) track slopes in data. Tracks are built using the Hough transform method.

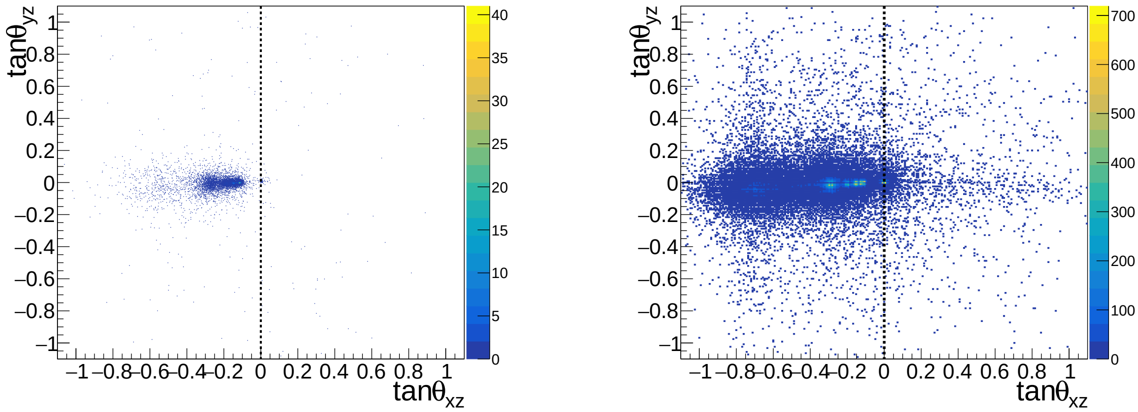

(a) (b)

Figure 26: SciFi (a) and DS (b) track slopes for data events in sync with B2noB1 LHC bunches. Tracks are built using the Hough transform.

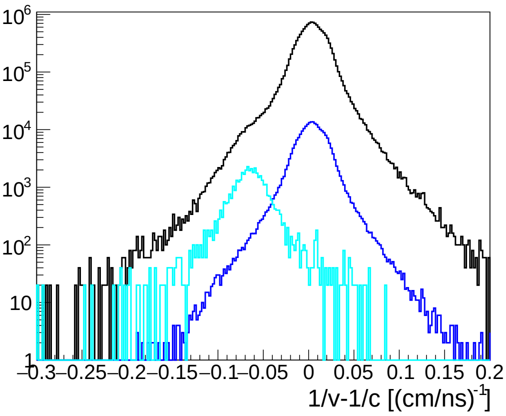

Figure 27: Track separation by particle propagation direction using simple tracking SciFi tracks. The black curve shows tracks reconstructed in all events. The blue distribution is for tracks in events of B1noB2 bunches and the cyan one - for events in B2noB1 bunches. Tracks of particles moving from the DS side towards the SciFi, dubbed backward-going, must have 1/v - 1/c values around -2/c or -0.067 $(\mathrm{cm/ns})^{-1}$.

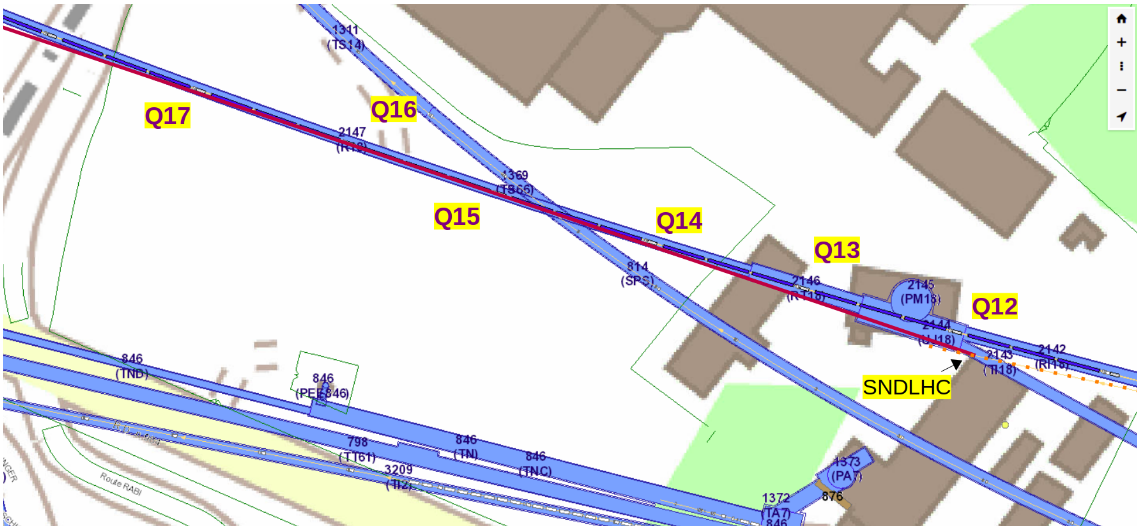

Figure 28: Map of the LHC area around the SND@LHC location. The abbreviations of the quadrupole magnets downstream of the detector are highlighted in yellow. The quadrupoles numbers correspond to the LHC half-cells of the same number. The original image is from the CERN GIS portal [24].

plane.

8 Muon flux

The flux of reconstructed muon tracks in the detector is estimated for two selected LHC fills, as discussed in Section 3. The muon flux is determined as the number of reconstructed tracks in a given SND@LHC run per corresponding IP1 integrated luminosity and unit detector area. Selected events are during "Stable beams" operation of the LHC and IP1 colliding bunches. IP1 collisions might coincide in time with other activity in the accelerator. The LHC bunch structure with respect to the SND@LHC detector is shown in Figure 31 for the two selected runs. Most bunch protons survive the IP beam crossings. At the SND@LHC location, IP1 collisions and the circulation of the remaining protons of the same IP1 colliding Beam 1 bunch are always synchronous. Independent of the presence of a bunch crossing and while moving towards the SND@LHC detector, if Beam 1 interacts in the beamline outside the IP1 collision area, the outgoing produced particles might leave a reconstructible trace in the apparatus. Further, IP1 colliding bunches sometimes coincide with other non-colliding bunches of Beam 2 circulating in the ring. In this cases, Beam 2 can interact with the beamline elements, producing particles that impinge on the detector. Lastly, IP1 colliding bunches are often in sync with the crossing of a different bunch pair at IP2. Figure 31a shows little difference in event rates between circulation of non-colliding Beam 2 bunches and IP2 collisions. Therefore, the particle contribution from IP2 collisions in the detector is considered negligible.

The number of muons associated with non-IP1 sources is determined in two cases: non-colliding Beam 1 bunches and Beam 2 no Beam 1 LHC bunches, noted B2noB1

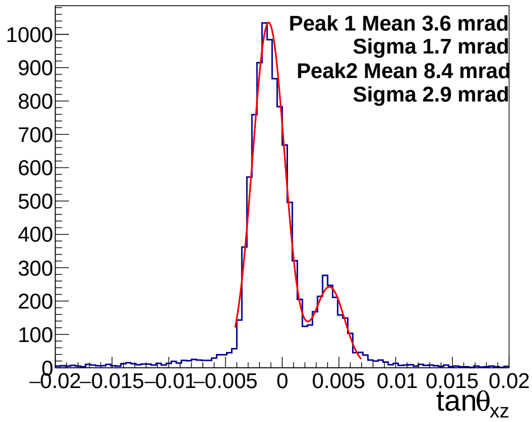

Figure 29: Data SciFi track slopes in the horizontal plane. The region around a few milliradian is selected to show the two central sub-peaks of the main peak. A double Gaussian is used to fit the peaks. The mean and sigma values of the global fit are reported.

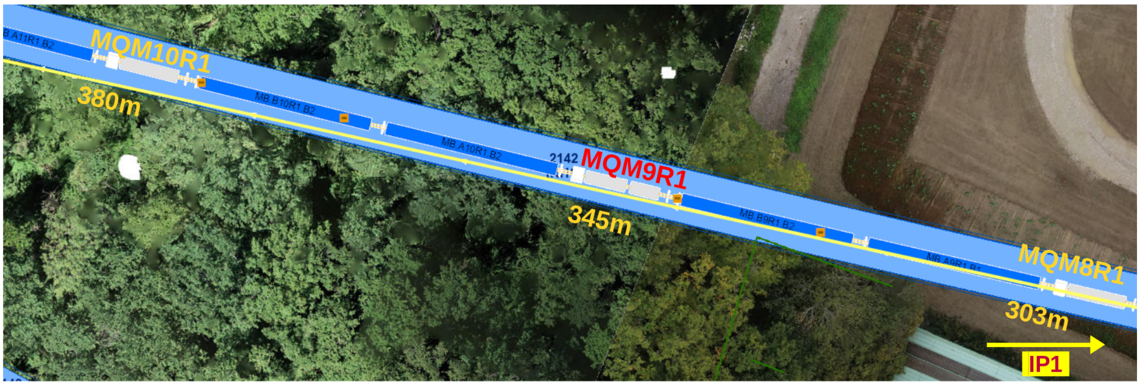

Figure 30: Map of the LHC area where Beam 1, the clock-wise circulating beam moving from right to left in this figure, is bent in the LHC arc at half-cell 9. The light yellow line shows the ATLAS detector axis. Abbreviations denote the quadruple magnets of the corresponding half-cells. The marked distances are with respect to IP1. The latter lies further on the left, outside of the map. The original image is from the CERN GIS portal [24].

for shortness. The latter accounts for particles entering the detector, but produced in Beam 2 interactions with the residual gas and the LHC machine elements. Once the number of muons per bunch in non-IP1 bunches is obtained, the contributions of Beam 1 and Beam 2 on the SND@LHC muon rate is subtracted from the number of reconstructed muons in IP1 colliding bunches. The following formula is used

$$N_{\mu\, IP1Only} = N_{\mu\, IP1} - \frac{N_{\mu\, B1Only}}{N_{B1Only}} \times N_{IP1\&B1} - \frac{N_{\mu\, B2noB1}}{N_{B2noB1}} \times N_{IP1\&B2}, \quad (5)$$

where N_μ is the number of reconstructed muon tracks and N is the number of bunches having the designated structure. Equation 5 implies an equal number of protons, equal beam current and dimensions per bunch.

The signal and background levels for the muon flux measurement are reported in Table 5 for the two selected fills. The filling scheme for fill 8297 is known to reduce beam-gas interactions, see Section 3. In terms of muons at the SND@LHC detector location, the observed reduction in the background levels associated with non-colliding Beam 1 and B2noB1 bunches is between 25 to 50 % depending on the detector system and the bunch type.

system	IP1 all [%]	IP1 collisions [%]	B1Only [%]	B2noB1 [%]
run 4705, LHC fill 8088				
SciFi	100	98.6	1.2	0.2
DS	100	98.5	1.1	0.4
run 5086, LHC fill 8297				
SciFi	100	99.2	0.7	0.1
DS	100	99.1	0.6	0.3

Table 5: Fractions of events associated with IP1 collisions, non-colliding Beam 1 and B2noB1 bunches for the two selected LHC fills. The filling scheme in fill 8297 suppresses the formation of electron cloud and reduces beam-gas interactions [7].

After corrections for Beam 1 and Beam 2 contributions, the data-based tracking efficiency correction, reported in Table 4, is applied. The correction is defined as the inverse of the efficiency. This is done for both selected runs, for SciFi and DS tracks built using both SND@LHC tracking approaches. The corresponding muon flux values are reported in Table 6. As expected, the DS muon flux is larger than the SciFi one, given the non-uniform flux in the vertical direction and the difference in the system's geometrical acceptance. Then, there are a few percent variations in the results per detector when comparing estimates for different tracking methods. Using simulations, it is demonstrated in Figures 16-17 that as a consequence of the presence of heavy material between tracking stations, the tracking performance of the two algorithms is not identical in different energy spectrum intervals. Since the muon flux results for the two tracking algorithms vary more than multiple times the statistical uncertainty, the dependence of the tracking performance on the muon energy is considered a muon flux systematic uncertainty source.

The central value of the final muon flux result per detector is the average of the calculated fluxes for the two SND@LHC runs when using the Hough transform

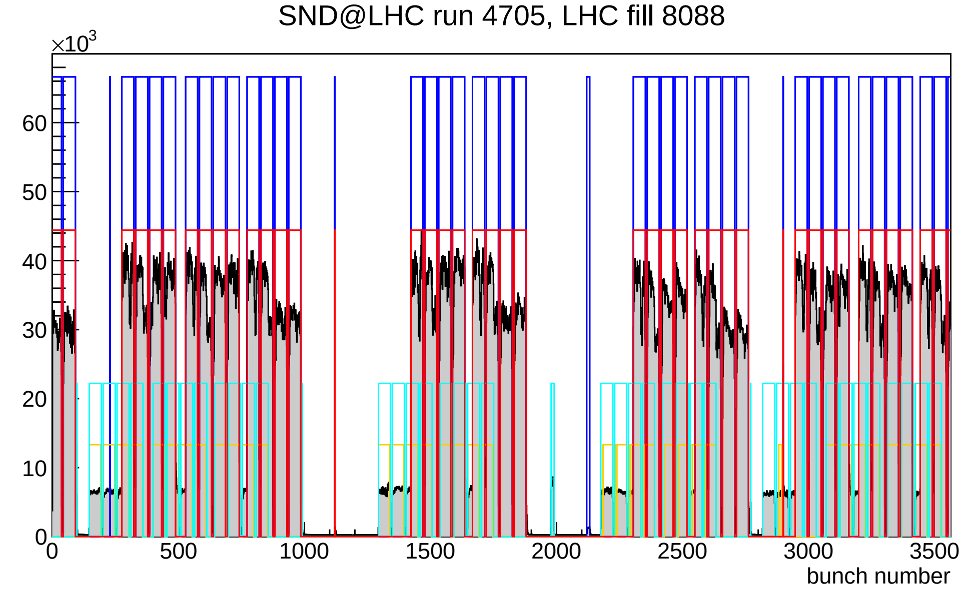

(a)

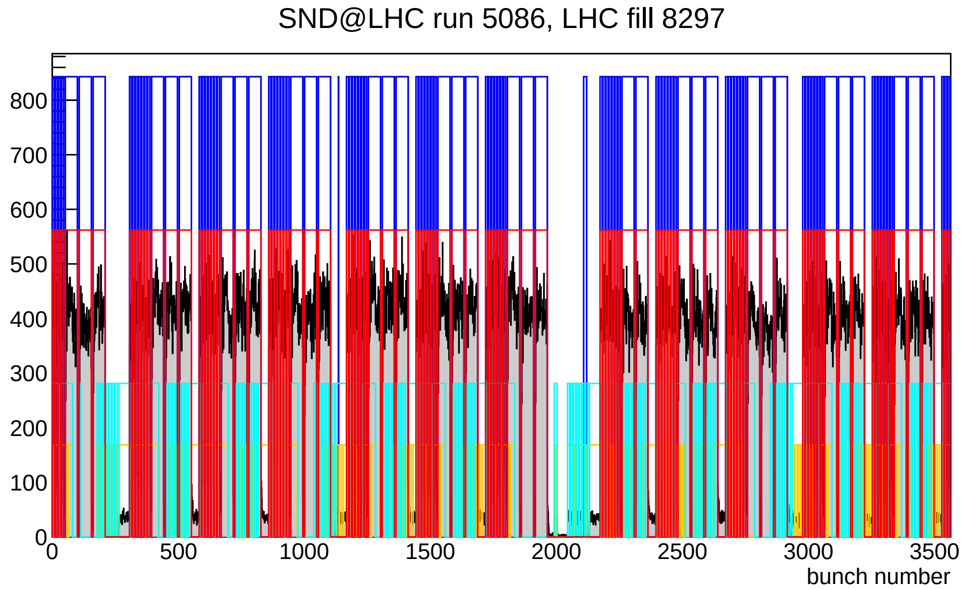

(b)

Figure 31: Bunch structure for LHC fill 8088, SND@LHC run 4705 (a) and LHC fill 8297, SND@LHC run 5086 (b). The black distribution on each plot is the SND@LHC event rate. The red boxes show bunches associated with Beam 1, the cyan ones - with Beam 2, the blue ones - IP1(ATLAS) collisions, the dark yellow ones - IP2(ALICE) collisions. The difference between the phase adjustments with respect to the SND@LHC clock of Beam 1 and of Beam 2 is 129 bunch numbers and corresponds to twice the distance from the detector to IP1.

tracking. The reason HT is selected is to maximize the tracking efficiency, thus minimize the correction. The integrated luminosity for a LHC fill is used to normalize the muon flux and the uncertainty of the former is propagated to the flux result. The ATLAS collaboration reports a 2.2% uncertainty in the integrated luminosity for data recorded in 2022 [25]. Additionally, since the tracking efficiency directly enters the muon flux estimate as a correction factor, a systematic uncertainty is attributed to its assessment. The uncertainty of the efficiency evaluation is taken as triple the standard deviation of tracking efficiency values over $1{\times}1$ cm^2 $x - y$ detector coordinate bins, see Table 4. For each systematic uncertainty source, separate flux estimates are calculated using one varied parameter at a time: tracking efficiency value, integrated luminosity or using the simple tracking. The deviations of those flux estimates from the central one are added in quadrature to form the total systematic uncertainty.

The muon flux is estimated in the selected SciFi inner fiducial volume between $-42\,\text{cm} \leq x \leq -11\,\text{cm}$ and $18\,\text{cm} \leq y \leq 49\,\text{cm}$. It defines a $31{\times}31$ cm^2 central detector area, rejecting regions of non-uniform detector efficiency, see Section 6.4.1. For the DS, the selected area is $52{\times}52$ cm^2, ranging between $-54\,\text{cm} \leq x \leq -2\,\text{cm}$ and $12\,\text{cm} \leq y \leq 64\,\text{cm}$. The SciFi and the DS muon flux estimates in the so-defined areas with statistical and systematic uncertainties are reported in Table 7. The total relative uncertainty of the flux results is 5 % for the SciFi measurement and 3 % for the DS one.

system	tracking algorithm	muon flux [10^4 fb/cm^2]
run 4705, LHC fill 8088		
SciFi	simple tracking	2.20 ± 0.01
	Hough transform	2.05 ± 0.01
DS	simple tracking	2.43 ± 0.01
	Hough transform	2.38 ± 0.01
run 5086, LHC fill 8297		
SciFi	simple tracking	2.20 ± 0.01
	Hough transform	2.06 ± 0.01
DS	simple tracking	2.41 ± 0.01
	Hough transform	2.34 ± 0.01

Table 6: Muon flux in two selected SND@LHC runs and LHC fills. Estimates with SciFi and DS data tracks built using simple tracking and the Hough transform are reported separately. The statistical uncertainty for each case is quoted. The considered detector fiducial volumes are defined in the text.

The SciFi and the DS muon flux measurements are compared restricting the DS fiducial volume to the one used for the SciFi measurement. The muon flux for both detectors in an area between $-42\,\text{cm} \leq x \leq -11\,\text{cm}$ and $18\,\text{cm} \leq y \leq 49\,\text{cm}$ is reported in Table 8. The relative difference between the two detector measurements

system	muon flux [10^4 fb/cm^2]
SciFi	$2.06 \pm 0.01 \pm 0.11$
DS	$2.35 \pm 0.01 \pm 0.08$

Table 7: Muon flux in the SciFi and the DS detectors of the SND@LHC experiment. Statistical and systematic uncertainties are reported. The considered systematic uncertainty sources are the uncertainty of the luminosity measurement, the slight fluctuations in tracking efficiency in different $x-y$ detector regions, and the dependence of the tracking performance on the muon energy. The considered detector fiducial volumes are defined in the text.

is 2%. It is smaller than the total relative uncertainty of each detector measurement, which is 5 % for the SciFi and 3 % for the DS measurement. The difference in the DS flux results in Tables 7 and 8 for the two different transverse $x-y$ detector regions is due to a flux gradient with the vertical y position and is discussed in the following Section 9.

system	muon flux [10^4 fb/cm^2] *same fiducial area*
SciFi	$2.06 \pm 0.01 \pm 0.11$
DS	$2.02 \pm 0.01 \pm 0.06$

Table 8: Muon flux in the SciFi and the DS detectors of the SND@LHC experiment considering identical detector fiducial area in range $-42\,\text{cm} \leq x \leq -11\,\text{cm}$ and $18\,\text{cm} \leq y \leq 49\,\text{cm}$. Statistical and systematic uncertainties are reported. The considered systematic uncertainty sources are the uncertainty of the luminosity measurement, the slight fluctuations of tracking efficiency in different $x-y$ detector regions, and the dependence of the tracking performance on the muon energy.

9 Data/MC simulation comparison

Having a muon flux data estimate, one can compare it with the value predicted by simulations. This comparison is done for the two available sets of Fluka simulations discussed in Section 4 and outlined in Table 2. It is not only the flux as a number that is to be compared. Important features such as the vertical flux gradient and the two neighboring peaks forming the main IP1 muon peak are to be sought in the Monte Carlo simulation as well.

In terms of muon flux, the two MC simulation sets provide expectations with a factor of 2 difference. The reason is the improved description of the experimental conditions, i.e., magnetic field extension, crossing angle, and TCL6 collimator settings, used to generate the March 2023 set. In Table 9 the MC simulation muon fluxes are reported for both sets and in two scenarios. One is the primary muon reaches the detector, and the other - the muon leaves a reconstructible trace in the detector. The difference between these two cases is due to the absorption of soft muons in the heavy material between tracking planes, the potential failure of track reconstruction if a shower evolves, or muon deep inelastic scattering. Particles going close to the detector edge or entering the volumes at large angles contribute to a lesser extent. The reasons are that the selected fiducial volume is in the inner part of the detector, and most muons from IP1 that reach the detector have milliradian angles. Overall, the difference in the expected muon fluxes for the two scenarios is below 2% for both systems.

system	number of MC points	muon flux [10^4 fb/cm^2]
March 2022 MC simulation set		
SciFi	1	4.29 ± 0.38
	3H +3V	4.28 ± 0.38
DS	1	4.41 ± 0.22
	3H +3V	4.36 ± 0.22
March 2023 MC simulation set		
SciFi	1	1.61 ± 0.05
	3H +3V	1.60 ± 0.05
DS	1	1.82 ± 0.03
	3H +3V	1.79 ± 0.03

Table 9: Generator muon fluxes in the SciFi and the DS selected fiducial ranges, $-42\,\text{cm} \leq x \leq -11\,\text{cm}$ and $18\,\text{cm} \leq y \leq 49\,\text{cm}$ for SciFi, and $-54\,\text{cm} \leq x \leq -2\,\text{cm}$ and $12\,\text{cm} \leq y \leq 64\,\text{cm}$ for DS. The fluxes are estimated for two scenarios. One case is the generated primary muon makes at least 1 MC point in a detector. The other, the muon leaves points in at least 3 horizontal(H) and 3 vertical(V) detector planes, i.e. it leaves a reconstructible trace. The statistical uncertainty for each case is quoted. As expected, it decreases with increased MC simulation statistics.

The simulation that better reflects the beam crossing angle for the year 2022 LHC run and features an extended magnetic field map and the correct TCL6 aperture setting, the March 2023 one, provides a prediction that is closer to the data observation. In Table 10 data flux estimations and results for that simulation sample are compared in two cases. In the first one, the data muon flux with data-based tracking efficiency correction is examined across an estimate of the muon flux for generated reconstructible muons. In the second case, the data muon flux without tracking efficiency correction is compared to the MC simulation muon flux estimated using reconstructed MC tracks. For the latter, the Hough transform tracking is used. In all cases, the muon flux estimates for data and simulations differ between 20-25 %.

The assessed systematic uncertainty of the MC simulation flux prediction is reported in Table 10. The considered sources relate to the Geant4 particle propagation simulation stage. Assessment of the Fluka sample uncertainty is not included. The evaluated systematic uncertainty factors are the composition of the rock between the scoring plane and the TI-18 tunnel and the precision of the relative alignment between the scoring plane and the SND@LHC apparatus. Originally, the standard FLUKA rock model is used in the GEANT4 particle propagation stage. The density of the material is 2.0 g/cm^3. As an alternative rock composition description, the FLUKA definition of Molasse rock with a density of 2.4 g/cm^3 has been employed since a recent study shows it represents well the actual rock surrounding the LHC envelope [26]. To address the uncertainty due to the scoring plane's relative alignment to the detector, the whole plane has been moved along the Z axis by $\pm$10 cm with respect to its nominal position. For each varied parameter, rock model, Z position of the scoring plane, a new simulation set has been generated and the MC analysis has been repeated. The total systematic uncertainty is the quadrature sum of the deviations of the new flux estimates with respect to the central one. Its magnitude is about 10% of the predicted flux value.

system	sample	muon flux [10^4 fb/cm^2]	1 - $\frac{\text{simulation}}{\text{data}}$ [%]
on the level of eff. corrected data and generator MC flux			
SciFi	data	$2.06 \pm 0.01 \pm 0.11$	22 ± 10
	simulation	$1.60 \pm 0.05 \pm 0.19$	
DS	data	$2.35 \pm 0.01 \pm 0.08$	24 ± 7
	simulation	$1.79 \pm 0.03 \pm 0.15$	
on the level of reconstructed tracks, no eff. corrections			
SciFi	data	$1.97 \pm 0.01 \pm 0.05$	23 ± 9
	simulation	$1.52 \pm 0.05 \pm 0.17$	
DS	data	$2.22 \pm 0.01 \pm 0.05$	21 ± 8
	simulation	$1.75 \pm 0.03 \pm 0.16$	

Table 10: Data/Monte Carlo simulation muon flux comparisons for SciFi and DS selected fiducial ranges. First, data muon flux with data-based tracking efficiency correction and the muon flux for generated reconstructible muons are reported. Second, the data muon flux without tracking efficiency correction and the MC simulation muon flux obtained using Hough transform MC reconstructed tracks are compared. The statistical and systematic uncertainties for each case are quoted. The agreement level between data and simulations and its total uncertainty are given in the last column.

The muon flux gradient with vertical position is evident in the SciFi and the DS data, which is shown in Figures 32a-b. However, the number of muons reaching the detector in as many as 200M simulated proton-proton interactions is insufficient to reproduce the vertical flux gradient in 2 dimensional(2D) $x - y$ bins, but the trend is clearly visible when one integrates over the x dimention. This is demonstrated in Figures 32c-f for the 2D case, where the March 2023 MC simulation is the single one that partially reflects the DS muon flux increase going to higher y positions. On the other hand, the SciFi and the DS 1D track distributions in y coordinate bins, presented in Figure 33 for the March 2023 set, do show an increased flux for larger y values.

It is reported in Section 7 that the electronic detectors data reveal a two-headed central peak in the horizontal muon track slopes distribution. For the March 2023 simulation sample, the distribution of the same parameter is shown in Figure 34. The two sub-peaks are present in the MC simulation as well, the distance between them being 5.5 mrad. This value is well compatible with the emulsion and electronic detectors data measurement of 5 mrad. The microradian shift of the absolute values of the peaks in MC simulation with respect to the data is to be further investigated. A possible reason can be the difference between actual geometry and the MC simulation geometry description induced by survey measurements' finite precision.

10 Conclusions

The muon flux at the SND@LHC detector location in the TI-18 tunnel has been assessed using the first data collected by the experiment during the LHC Run 3 operation in 2022. Results using the information provided by the two independent electronic detector systems, the fine-granulated SciFi and the DS, are reported. The measured muon flux using the SciFi is $2.06 \pm 0.01(\text{stat}) \pm 0.11(\text{sys}) \times 10^4\,\text{fb/cm}^2$, while for the DS it is $2.35 \pm 0.01(\text{stat}) \pm 0.08(\text{sys}) \times 10^4\,\text{fb/cm}^2$. The total relative uncertainty of the results is 5 % for the SciFi and 3 % for the DS measurement. The statistical uncertainties are rather low given the large analysis data sample. In a single LHC fill, tens of millions of muons go through the detector. The reported systematic uncertainty takes into account the dependence of the tracking performance on the muon energy, respectively the tracking method used, the uncertainty of the luminosity measurement, and the slight fluctuations in tracking efficiency in different $x - y$ detector regions. Data/Monte Carlo simulation comparisons are also reported. The predicted MC simulation muon flux in each detector is 20-25 % lower than the measured one. The simulation prediction is assigned about 10 % relative systematic uncertainty, not including the one of the FLUKA muon flux at the scoring plane. The assessed systematic uncertainty of the MC simulation prediction is associated with the GEANT4 particle propagation simulation stage and accounts for rock modeling and alignment between the scoring plane and the detector.

Detector calibration, track reconstruction and tuning, and a thorough study of the LHC filling scheme have been successfully performed and assist all analyses. Furthermore, essential inputs for the flux measurement are the LHC accelerator status and luminosity information. Consistent results for the origins of tracks entering the detector from different sides, e.g. IP1, the back or sides of the detector, are provided using the angular track distribution in the horizontal plane, the detector hit timing, and the LHC bunch structure information. The vast majority of muons originate in IP1 collisions. A small fraction of tracks, synchronous to Beam 2 presence in the area, impinge on the SciFi and the DS from the back or the sides. Their contribution to the muon flux has been assessed and subtracted from the selected data sample.

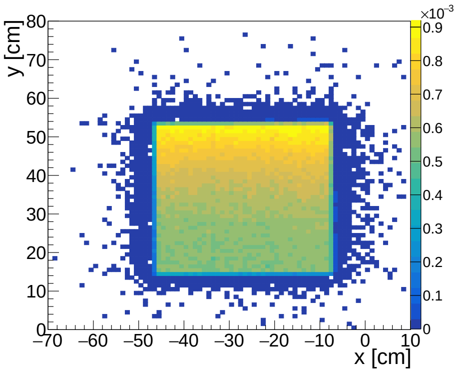

(a)

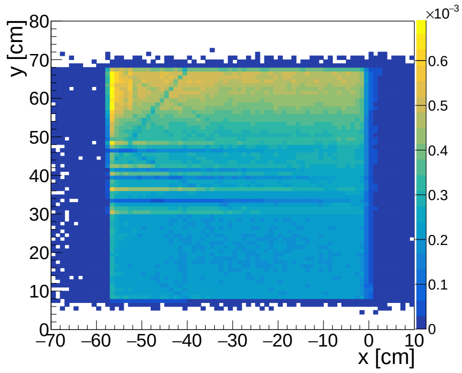

(b)

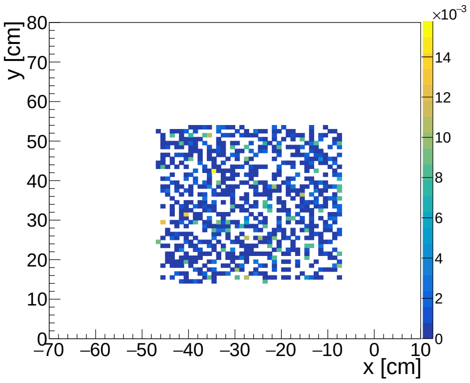

(c)

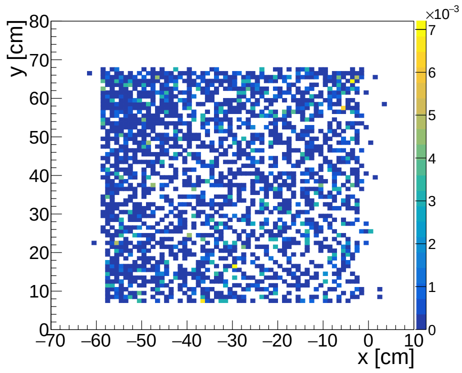

(d)

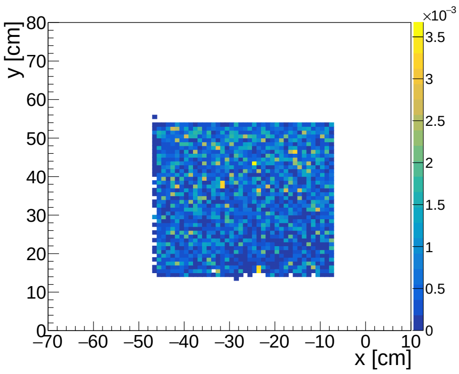

(e)

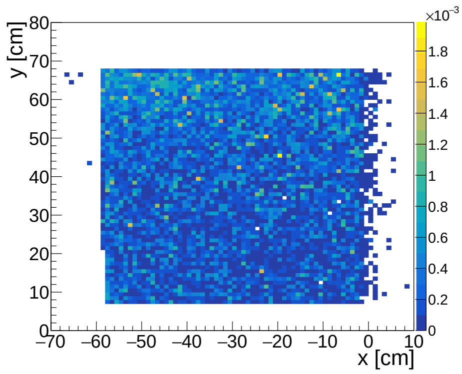

(f)

Figure 32: Reconstructed tracks $x - y$ profile at the upstream detector face for SciFi and DS tracks for data and simulations. Tracks are built using the Hough transform tracking. The data $x - y$ profiles in SciFi (a) and in DS (b) show an increase in the muon flux with vertical y position. It is not observed in the March 2022 MC simulation sample (c) - (d). For the March 2023 sample, the SciFi profile (e) is rather uniform, while there is a slight vertical gradient for the DS (f). Each distribution is normalized to unit integral.

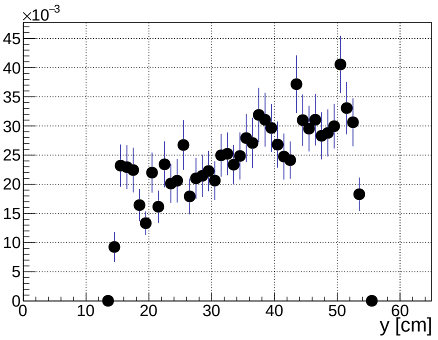

(a)

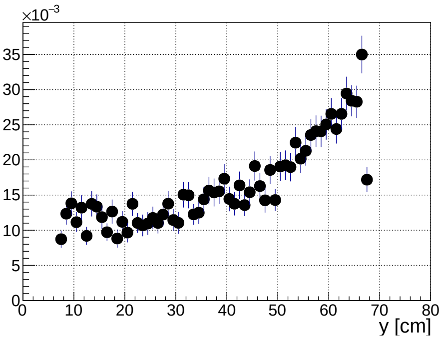

(b)

Figure 33: Normalized numbers of reconstructed tracks in vertical y position bins at the upstream detector face for SciFi (a) and DS (b) tracks using the March 2023 MC simulation set. Tracks are built using the Hough transform tracking. For each system, the muon flux increases towards the top of the detector. The two distributions are normalized to unit integral.

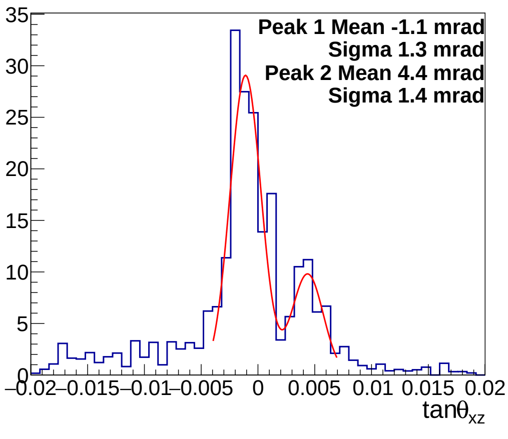

Figure 34: MC muon track slopes in the horizontal plane. The region around a few milliradians is magnified to show the two central sub-peaks of the main peak. A double Gaussian is used to fit the peaks. The means and sigmas of the global fit are reported.

A number of effects have been studied, verified between electronic detectors and emulsion data, and cross-examined with simulations. A closer look at the horizontal angular peak for muons penetrating the SciFi tracker reveals a two sub-peak structure. The two peaks are also present in emulsion data and in MC simulation. The distance between them in all cases is about 5 mrad. A point source cannot be assigned to the muons forming the secondary peak. They are produced in the follow-up of IP1 proton-proton collisions along the path from the IP to the SND@LHC apparatus.

In the data, there is a well-pronounced gradient of the muon flux with the vertical position for both SciFi and DS. The available simulation statistics are sufficient to reproduce this effect when integrating over the horizontal x positions. Additionally, preliminary emulsion data results show the same vertical structure in the emulsion tracks density.

The current note provides a detailed overview of the first measurement of the muon flux with the SND@LHC electronic detectors. The measured muon flux is used to constrain the muon-induced background in neutrino searches.

References

[1] **SND@LHC** Collaboration, C. Ahdida et al., “SND@LHC - Scattering and Neutrino Detector at the LHC.” https://cds.cern.ch/record/2750060, 2021.

[2] O. S. Brüning, P. Collier, P. Lebrun, S. Myers, R. Ostojic, J. Poole, and P. Proudlock, *LHC Design Report*. CERN Yellow Reports: Monographs. CERN, Geneva, 2004.

[3] “LHC Programme Coordination.” https://lpc.web.cern.ch/. Accessed April 2023.

[4] R. Lauckner, *LHC Operational Modes*, *LHC-OP-ES-0004* (2004).

[5] **ATLAS** Collaboration, M. Aaboud et al., *Luminosity determination in pp collisions at* $\sqrt{s}$ *= 8 TeV using the ATLAS detector at the LHC*, *Eur. Phys. J. C* **76** (2016), no. 12 653, [arXiv:1608.03953].

[6] **ATLAS** Collaboration, *Luminosity determination in pp collisions at* $\sqrt{s} = 13$ *TeV using the ATLAS detector at the LHC*, [arXiv:2212.09379].

[7] G. Iadarola, H. Bartosik, E. Belli, L. R. Carver, P. Dijkstal, K. S. B. Li, L. Mether, A. Romano, and G. Rumolo, *MD421: Electron cloud studies on 25 ns beam variants (BCMS, 8b+4e)*, 2017. https://cds.cern.ch/record/2260998.

[8] A. Iuliano, *Measurement of the muon flux with the emulsion target at SND@LHC*, 2023. in preparation.

[9] G. Battistoni et al., *Overview of the FLUKA code*, *Annals Nucl. Energy* **82** (2015) 10–18.

[10] C. Ahdida et al., *New Capabilities of the FLUKA Multi-Purpose Code*, *Front. in Phys.* **9** (2022) 788253.

[11] S. Roesler, R. Engel, and J. Ranft, *The Monte Carlo event generator DPMJET-III*, in *International Conference on Advanced Monte Carlo for Radiation Physics, Particle Transport Simulation and Applications (MC 2000)*, pp. 1033–1038, 12, 2000. [hep-ph/0012252].

[12] A. Fedynitch, *Cascade equations and hadronic interactions at very high energies*. PhD thesis, KIT, Karlsruhe, Dept. Phys., 11, 2015.

[13] A. Lechner et al., *Validation of energy deposition simulations for proton and heavy ion losses in the CERN Large Hadron Collider*, *Phys. Rev. Accel. Beams* **22** (2019), no. 7 071003.

[14] D. Prelipcean, K. Biłko, F. Cerutti, A. Ciccotelli, D. Di Francesca, R. García Alía, B. Humann, G. Lerner, D. Ricci, and M. Sabaté-Gilarte, *Comparison Between Run 2 TID Measurements and FLUKA Simulations in the CERN LHC Tunnel of the Atlas Insertion Region*, *JACoW IPAC* **2022** (2022) 732–735. http://cds.cern.ch/record/2839993.

[15] **GEANT4** Collaboration, S. Agostinelli et al., *GEANT4–a simulation toolkit*, *Nucl. Instrum. Meth. A* **506** (2003) 250–303.

[16] **SND@LHC** Collaboration, G. Acampora et al., *SND@LHC: The Scattering and Neutrino Detector at the LHC*, [arXiv:2210.02784]. https://cds.cern.ch/record/2838901.

[17] "SND@LHC survey measurements." https://edms.cern.ch/document/2882720/1/.

[18] P. V. Hough, *Method and means for recognizing complex patterns*, *U.S. Patent 30696541962* (1962).

[19] V. F. Leavers, *Computer Vision: Shape Detection*, pp. 1–18. Springer London, London, 1992.

[20] R. E. Kalman, *A New Approach to Linear Filtering and Prediction Problems*, *Journal of Basic Engineering* **82** (03, 1960) 35–45.

[21] R. Fruhwirth, *Application of Kalman filtering to track and vertex fitting*, *Nucl. Instrum. Meth. A* **262** (1987) 444–450.

[22] J. Rauch and T. Schlüter, *GENFIT — a Generic Track-Fitting Toolkit*, *J. Phys. Conf. Ser.* **608** (2015), no. 1 012042, [arXiv:1410.3698].

[23] C. Höppner, S. Neubert, B. Ketzer, and S. Paul, *A novel generic framework for track fitting in complex detector systems*, *Nuclear Instruments and Methods in Physics Research Section A: Accelerators, Spectrometers, Detectors and Associated Equipment* **620** (2010), no. 2 518–525.

[24] "CERN GIS Portal." https://gis.cern.ch. Accessed April 2023.

[25] **ATLAS** Collaboration, *Preliminary analysis of the luminosity calibration of the ATLAS 13.6 TeV data recorded in 2022*, tech. rep., CERN, Geneva, 2023. All figures including auxiliary figures are available at https://atlas.web.cern.ch/Atlas/GROUPS/PHYSICS/PUBNOTES/ATL-DAPR-PUB-2023-001.

[26] M. Tisi, A. Infantino, and P. Dyrcz, "HL-LHC cores drilling: summary of HSE-RP studies and recommendations." https://edms.cern.ch/document/2861462/2/approvalAndComments. Presentation given to the HL-LHC WP15 Integration Meeting held on March 24, 2023.